RAI Volume 3, Chapter 2.2.1.3.6, Second Set, Number 2:

> Explain how the temperatures predicted by the Multiscale Thermohydrological Model (MSTHM) results (SAR Section 2.3.5.4.1.3.2) used in TSPA are representative of the thermal response derived from the anticipated range of thermal loading (SAR Section 2.3.5.4.3, and SNL, 2008a, Section 6.4.2). This information is needed to determine compliance with 10 CFR 63.114(a)(2).
>
> Basis: It is not transparent how the temperatures predicted in SNL 2008a (Figures 6-4.2-1 through 6.4.2-15) fit into the range of MSTHM results (SNL, 2008b, Figure 2.3.5-33). The thermohydrologic responses to the selected hottest loading conditions (7- and 3-point segments from the 96/2 emplacement sequence) are compared to the results from two-dimensional and three-dimensional submodels of the MSTHM (SNL, 2008a, Section 6.4.2). The minimum drift wall and waste package temperatures for the 3-point case are below boiling at all times (SNL 2008a, Figures 6.4.2-10(a), 6.4.2-12(a) and 6.4.2-14(a)) for the cases considered in the analysis. This suggests that the lower bound temperatures expected at the repository are lower than those predicted by the MSTHM model (SAR Figure 2.3.5-33). In addition, the fraction of the repository that will have Case 2 (3-point segment) type of waste packages was not found.
>
> It is not clear how much the difference between results from the MSTHM (SNL, 2008b) and results of thermohydrologic response to the design heat load (SAR, Section 2.3.5.4.3, and SNL, 2008a, Section 6.4.2) is caused by the input parameters of heat load, ventilation efficiency, and heat load emplacement strategy. The heat load discussed in SNL (2008a, Section 6.4.2) states that after 100 years the linear heat load is very similar to the heat load used in MSTHM (SNL, 2008b). The readme file associated with this DTN (MO0705SUPPCALC.000) indicates a three-term exponential fit to the average line load for the postclosure thermal reference case is being calculated. It is not clear what heat load (exponential fit or actual heat load) was used to compare the results. The description provided in SNL (2008a) also is not clear about the quantitative impact of ventilation on heat load. Additionally, the heat load used to represent the base case in 3-D Model Analysis of Temperature Range (SNL, 2008a, Section 6.4.2.3) using the DDTH model is not clearly explained.

1. RESPONSE

The multiscale thermohydrologic model (MSTHM) results (SNL 2008a) are representative of the thermal response derived from the anticipated range of thermal loading because: (1) the range of predicted temperatures represents the effects of heating on postclosure performance; (2) waste package heat output used in the MSTHM is based on a reasonable description of the waste inventory (SNL 2007a); and (3) differences in predicted temperatures between the MSTHM and the postclosure analysis of the range of design thermal loading (SNL 2008b) are minor. The temperatures predicted for the range of design thermal loading (SNL 2008b, Sections 6.3 and 6.4.2) are not intended to fit into the range of the MSTHM results. The converse is true, the

MSTHM results fit into the range of temperatures for the anticipated range of design thermal loading.

The postclosure thermal loading analysis (SNL 2008b) was performed to further define the envelope of repository thermal conditions, by analyzing a representative waste stream incorporating the use of transportation, aging, and disposal canisters, and considering multiple waste type, spent fuel aging, and emplacement scenarios. The analysis selected an estimated limiting waste stream (ELWS), simulated the emplacement of the ELWS in the underground repository, and evaluated the geomechanical, geochemical, and hydrogeologic responses of the repository host rock to the resulting thermal loading conditions. Different emplacement strategies were compared, varying the target value for the running average of an index of waste package thermal energy density, and varying the capacity of surface storage described in terms of the number of years that waste receipts can be stored at the surface. The strategies compared consisted of: (1) 85ºC target mid-pillar temperature with four years initial surface capacity (85/4 emplacement sequence), and (2) 96ºC target mid-pillar temperature with two years initial surface capacity (96/2 emplacement sequence).

Note that the index of thermal energy density, or "thermal-energy-density index" (SAR Section 1.3.1.2.5), for a waste package is the local peak mid-pillar temperature if the nearby vicinity and drifts are loaded only with waste packages having the particular heat generation characteristics of the package. A running average of this index for successively emplaced waste packages then estimates the local peak mid-pillar temperature, accounting for local variability in heat generation of waste packages. A seven-package running average was shown to adequately represent the effect of package variability (SNL 2008b, Section 6.1).

The two emplacement sequence strategies are described in more detail in SAR Sections 1.3.1.2.5 and 2.3.5.4.3, and in *Postclosure Analysis of the Range of Design Thermal Loadings* (SNL 2008b, Section 6.1.3). Both strategies produced locally cooler and locally hotter conditions than those represented in the MSTHM model. The hotter conditions were further analyzed to confirm the validity of total system performance assessment (TSPA) supporting models, and both the hotter and cooler conditions were evaluated to verify that screening designation of features, events, and processes (FEPs) for the TSPA as included or excluded does not change (SAR Section 1.3.1.2.5; SNL 2008b, Section 6.5). The MSTHM results fit within the range of the hotter and cooler conditions generated for each of the two emplacement sequence strategies.

Importantly, an emplacement drift loading plan will be developed (SAR Section 1.3.1.2.5) for each drift, or set of drifts, with specific information describing the waste to be emplaced. The emplacement drift loading plan will specify waste characteristics, waste package emplacement locations, and ventilation duration, and it will show how preclosure and postclosure performance requirements will be met.

1.1 DISCUSSION OF TEMPERATURES CALCULATED FOR THE RANGE OF DESIGN THERMAL LOADING

In the postclosure thermal loading analysis, emplaced sequences of waste packages were simulated (85/4 and 96/2 sequences; SNL 2008b, Section 6.1.3), and the hottest local conditions in those sequences were identified for further analysis and comparison with thermal-hydrologic conditions simulated by the MSTHM and used in the TSPA. The hottest local conditions were selected using an estimate of the peak local drift wall temperature at each waste package (SNL 2008b, Section 6.1.4). To allow for the effect of thermal radiation, which transfers heat between adjacent waste packages, the hottest segments were selected based on three-package and seven-package running averages of the estimated peak drift wall temperature.

The selected hottest segments (three- and seven-package segments from the 96/2 emplacement sequence) were then simulated using two-dimensional and three-dimensional thermal-hydrologic models, and the resulting temperatures were compared to MSTHM base-case results for the corresponding infiltration and host-rock thermal conductivity conditions. The two-dimensional cases (SNL 2008b, Section 6.4.2.2) used the average line-loads for the 13 waste packages centered on the three- and seven-package segments, for comparison with two-dimensional calculations generated as intermediate results by the MSTHM. As noted in the analysis (SNL 2008b, Section 6.4.2.2), temperatures for the two-dimensional implementation of the seven-package case are similar to results from the two-dimensional, line-averaged-heat-source, mountain-scale, thermal-hydrologic submodel used in the MSTHM, because the line loads are similar. Some of the waste packages in the seven-package segment have greater heat output at emplacement than the hottest packages represented in the MSTHM, but the ventilation period is 72 years (SNL 2008b, Section 6.3) compared to 50 years assumed for the MSTHM.

The three-dimensional cases (SNL 2008b, Sections 6.4.2.3 and 6.4.2.4) represent a repeating segment of 13 waste packages, where the 13 packages are taken directly from the 96/2 emplacement sequence, centered on either the hottest three- or seven-package segment (SNL 2008b, Section 6.1.4). Representing three-dimensional drift-scale thermal-hydrology with discrete waste packages makes these discrete-heat-source, drift-scale, thermal-conduction submodel cases in the MSTHM terminology. The use of 13 packages makes these cases similar to the finite element calculations in the postclosure analysis of design thermal loading (SNL 2008b, Section 6.3), which analyzed the same three- and seven-package hottest segments (Scenarios 3 and 4, respectively). In the comparison figures (SNL 2008b, Figures 6.4.2-4 through 6.4.2-15), base-case MSTHM results calculated using the multiscale methodology with the unit-cell waste package arrangement used for the TSPA (SAR Section 2.3.5.4.1.3) are plotted for the same infiltration and host-rock thermal conductivity conditions used for the three- and seven-package cases (the P10, P10L, and P90 cases were selected). All of these three-dimensional calculations use lookup tables for waste package thermal output, which is based on the radionuclide inventory in each package and was calculated as part of the engineering study used as input (SNL 2008b, Section 4.1.1). The three-term exponential fit discussed in the RAI is used only for exposition of mid-pillar temperature behavior (SNL 2008b, p. 6-7) and not for calculating thermal energy density in the emplacement analysis.

After repository closure and the cessation of forced ventilation, waste package locations (including the package and the drift wall) will typically warm to above-boiling temperatures and remain so for up to approximately 1,500 years depending on proximity to the repository edge, local thermal loading, host-rock thermal conductivity, and percolation flux (SAR Section 2.3.5.4.1.3.2). Thermal-hydrologic simulations for an ELWS representing the range of anticipated thermal loading are comparable to simulations using the MSTHM unit-cell arrangement of waste packages throughout the repository, where the emplacement sequence intersperses commercial spent fuel and codisposal waste packages (SNL 2008b, Sections 6.3 and 6.4.2). The corresponding differences between temperatures simulated using the ELWS, and the MSTHM results, are quantitatively small. The geomechanical, hydrogeologic, and geochemical system responses are within the range of applicability and validation for the respective models (SNL 2008b, Section 6.4).

Maximum drift wall and waste package temperatures for individual waste package locations may be less than boiling, as shown in the three- and seven-package segment analysis (SNL 2008b, Sections 6.3.2.3, 6.3.2.4, and 6.4.2.3). This occurs where cooler codisposal waste packages are grouped together. Finite-element heat-transfer calculations showed that radiative coupling of heat in the axial direction, from hotter to cooler waste packages, extends only over a few waste package lengths (SNL 2008b, Section 6.3.2). Thus, any group of approximately four or more codisposal waste packages may produce sub-boiling local peak postclosure temperatures. The extent of such grouping depends on the thermal loading strategy, and will be determined in the emplacement drift loading plan (SAR Section 1.3.1.2.5). For example, in the 96/2 emplacement sequence, codisposal packages are well interspersed among the hotter spent fuel packages to limit the running average thermal energy density, and few codisposal packages are emplaced after the spent fuel is emplaced. By contrast, in the 85/4 sequence, the spent fuel packages are cooler (having been aged longer at the surface), and many codisposal packages are emplaced after the spent fuel is emplaced. The codisposal packages that are emplaced later form a long segment with mostly codisposal and few spent fuel packages.

The difference between simulated sub-boiling peak temperatures and the MSTHM results used in the TSPA is minor because cooler conditions attenuate thermally driven processes that affect the ambient state of the natural barriers. This relationship is supported by evaluation of FEPs affected by thermal loading (SNL 2008b, Section 6.5).

The average lineal heat load for the ELWS was determined by averaging the heat output of all waste packages, regardless of the emplacement sequence. The result is similar to the average line-load corresponding to the unit-cell used in the MSTHM (SAR Figure 1.3.1-6). The ELWS includes spent fuel waste packages that are hotter because of younger age out-of-reactor, higher burnup, or both. The similarity of average thermal output arises because of differences in ventilation duration as discussed above.

The major differences in peak temperatures among codisposal and spent fuel waste packages, and between the MSTHM results and the postclosure thermal loading analysis, are caused by grouping together cooler packages (i.e., local heat load is the predominant influence). Ventilation efficiency and duration could be increased to reduce the number of package locations where the boiling temperature is exceeded. However, previous analysis showed that boiling temperatures will occur in the repository where commercial spent fuel is emplaced, after preclosure ventilation for as long as 100 years (SNL 2007b, Section 7). The thermal emplacement strategy (SAR Section 1.3.1.2.5) limits the peak mid-pillar temperature but, with the ELWS realized for the postclosure thermal loading analysis, does not constrain peak postclosure in-drift temperatures to be less than boiling at all waste package locations.

In summary, the postclosure analysis of design thermal loading (SNL 2008b) evaluated geomechanical, geochemical, and hydrogeologic responses to the anticipated range of thermal loading conditions. Using simulation of the waste stream to be received at the repository, and its emplacement underground, the analysis identified local thermal conditions that range from slightly hotter to cooler than the MSTHM results used in the TSPA. In-drift thermal-hydrologic conditions predicted by the MSTHM are representative of this range. The geomechanical, hydrogeologic, and geochemical responses are within the range of applicability and validation for the respective models that support the TSPA (SNL 2008b, Section 6.4), and the screening of FEPs is not changed (SNL 2008b, Section 6.5). The analysis of design thermal loading also shows that the peak waste package and drift wall temperatures may be locally sub-boiling, but only where cooler (i.e., codisposal) waste packages are grouped together.

2. COMMITMENTS TO NRC

None.

3. DESCRIPTION OF PROPOSED LA CHANGE

None.

4. REFERENCES

SNL (Sandia National Laboratories) 2007a. *Initial Radionuclide Inventories*. ANL-WIS-MD-000020 REV 01 ADD 01 ACN 01. Las Vegas, Nevada: Sandia National Laboratories. ACC: DOC.20070801.0001; DOC.20050927.0005.

SNL 2007b. *Thermal Management Flexibility Analysis*. ANL-EBS-MD-000075 REV 01. Las Vegas, Nevada: Sandia National Laboratories. ACC: DOC.20070207.0001.

SNL 2008a. *Multiscale Thermohydrologic Model*. ANL-EBS-MD-000049 REV 03 ADD 02. Las Vegas, Nevada: Sandia National Laboratories. ACC: DOC.20080201.0003.

SNL 2008b. *Postclosure Analysis of the Range of Design Thermal Loadings*. ANL-NBS-HS-000057 REV 00. Las Vegas, Nevada: Sandia National Laboratories. ACC: DOC.20080121.0002: LLR 20080408.0252: DOC.20080828.0006.

RAI Volume 3, Chapter 2.2.1.3.6, Second Set, Number 3:

> Explain how the locations for injection tests used for calibration of the seepage model are representative of variability across the repository footprint. This information is needed to determine compliance with 10 CFR 63.114(a)(1,2).
>
> Basis: Ten injection zones along boreholes at several locations (4 for lithophysal and 2 for nonlithophysal rock) in the ESF and ECRB (SAR Table 2.3.2-2) are used to calibrate the ambient seepage model. No discussion is provided for why these locations are representative of the repository rock units, in terms of rock or hydrological properties. For example, fracture characteristics from the detailed line survey are extensively discussed for the conceptual and numerical model in SAR Section 2.3.3.2.3.2, but are not used in placing the injection zones, or locations, into a representative or variability context.

1. RESPONSE

The locations at which liquid release tests were conducted for calibration of the capillary-strength parameter used in the ambient seepage model were specifically selected to be representative of the spatial variability in fracture and lithophysal characteristics within the repository rock units. The seepage model was calibrated against seepage-rate data from liquid-release tests performed in several niches along the Exploratory Studies Facility (ESF) and the Enhanced Characterization of the Repository Block (ECRB) Cross-Drift. Detailed discussion of the selection and characteristics of these locations is given in *Abstraction of Drift Seepage* (SNL 2007, Section 6.6.2.2), *Seepage Calibration Model and Seepage Testing Data* (BSC 2004a, Section 6.5.1), and *In Situ Field Testing of Processes* (BSC 2004b, Sections 6.1.1.1 and 6.11). Uncertainty in spatial variability of this parameter, associated with variability in regions of the rock mass not accessed for testing, is estimated and incorporated in the seepage abstraction (SNL 2007, Section 6.6.2.3).

As noted in the RAI, calibrated capillary-strength values were developed for ten injection zones from six different test locations. The two niches used for calibration of the capillary-strength parameter in nonlithophysal units are Niche 3 (also named Niche 3107, referring to construction station 31+07) and Niche 4 (also named Niche 4788). The test locations were selected based on the different fracture characteristics of the Topopah Spring Tuff middle nonlithophysal (Tptpmn) unit exposed at these construction stations. Niche 3 consists of a 6.3-m-long drift located in an area of relatively low fracture density. Niche 4 consists of an 8.2-m-long drift located in the 950-m-long exposure of an intensely fractured zone in the Tptpmn unit. Fractures in this zone are not uniformly spaced, but instead occur in clusters of closely spaced fractures. Liquid release tests were also conducted in Niche 2 (also named Niche 3650), which consists of a 9-m-long drift located in rock exhibiting moderate fracture density. The capillary-strength values from the Niche 2 tests were not used for calibration because the testing methodology was considered less reliable due to the short test duration. The flow diversion and seepage behavior observed in the Niche 2 tests, however, was consistent with the tests conducted in Niches 3 and 4. Together, the three test locations are representative of the repository-scale variability of fracture conditions in the nonlithophysal zones along the ESF, ranging from relatively low to moderate to strong fracturing, comprising the range of conditions exposed in the detailed line survey. Multiple tests in several injection intervals were conducted in each niche, representing small-scale variability on the order of a few meters.

The calibration conducted for test locations in the lithophysal units used data from Niche 5 (also named Niche 1620), which consists of a 15.0-m-long drift located on the south side of the ECRB Cross-Drift in the Topopah Spring Tuff lower lithophysal (Tptpll) unit. This unit comprises many smaller fractures (less than 1 m long) interspersed with many lithophysal cavities, ranging in size from 1 cm to 180 cm (SNL 2007, Section 6.6.1.3; BSC 2004c, Appendix O). Additional data were used from liquid release tests conducted in three systematic-testing boreholes in the Tptpll unit, all about 20 m in length, drilled into the roof of the ECRB Cross-Drift (BSC 2004b, Section 6.11). The "systematic" approach refers to testing locations chosen at regular intervals. This approach complemented other hydrologic testing in which test locations were selected for specific geologic characteristics (such as the area of intense fracturing near Niche 4). Together, the data from Niche 5 and from the three systematic-testing boreholes are representative of the variability of geologic conditions in the lithophysal zones exposed along the ECRB Cross-Drift, with respect to fracture characteristics as well as the presence and geometric properties of lithophysae. For example, the Tptpll test locations are separated by a distance of approximately 150 m along the ECRB Cross-Drift, from construction station 16+20 (Niche 5) to almost 17+63 (where the passive bulkhead test interval begins). Comparison with the lithophysal abundance or porosity variation (comparing BSC 2004c, Section 6.1.4.2, Figure 6-12, with Appendix O, Figures O-9 through O-11) shows that the variability at 150-m intervals is similar to the variability along the entire ECRB (i.e., the apparent correlation length of lithophysal porosity, an important rock characteristic, is much smaller than 150 m, the spacing between test locations).

The calibrated capillary-strength parameter values are used in the seepage abstraction (SNL 2007, Section 6.6.2) to develop appropriate probability distributions for the total system performance assessment (TSPA) seepage calculations. These distributions represent the spatial variability of this parameter, and its related uncertainty, within the repository footprint. Even with careful selection of seepage test locations, uncertainty remains as to how well spatial variability within the repository footprint can be derived from the limited number of test locations available along the ESF and the ECRB. This uncertainty is discussed below.

It is important to recall the seepage calibration and modeling approach to evaluate the spatial variability of calibrated capillary strength from the data discussed above, and to recognize how this parameter is related to the fracture and lithophysal characteristics of the rock units. In capillary theory, the capillary-strength parameter represents the capillary behavior of a porous medium. Thus, in theory, this parameter could vary considerably between rock units that may have different capillary behavior due to differences in fracture and lithophysal characteristics, such as the lithophysal and nonlithophysal rock units at Yucca Mountain. However, the ambient seepage models used in the TSPA seepage calculations derive and apply capillary strength as an effective process parameter that accounts for a number of other factors in addition to capillary behavior (BSC 2004a, Section 6.3.3.2). Some of these factors (e.g., drift-wall roughness, film flow along drift wall, artifacts of discretization) are largely independent of fracture and lithophysal characteristics. Consequently, the calibrated capillary-strength parameter is not strongly correlated to the observed spatial variability in rock properties between different seepage test locations. In other words, this parameter is expected to exhibit less variation between and within geologic units as compared to other rock characteristics such as the fracture network permeability. It was concluded, based on a comparison of different statistical measures, that the spatial variability distribution for capillary strength could be developed without distinguishing between lithophysal and nonlithophysal units (SNL 2007, Section 6.6.2.2). Further justification for spatial uniformity of the spatial uncertainty and variability distribution used to represent capillary strength in the seepage abstraction for the TSPA, is provided in the response to RAI 3.2.2.1.3.6-2-004.

The probability distributions developed in the seepage abstraction (SNL 2007, Section 6.2) adequately account for the spatial variability and uncertainty of the capillary-strength parameter within the repository rock units. These distributions, described separately for spatial variability and uncertainty, are sampled in the TSPA seepage calculation to interpolate seepage rates from pre-computed lookup tables. The spatial variability of the capillary-strength parameter is given by a uniform distribution, with the minimum and maximum values defined by the statistics (mean, standard deviation) of the sample. The spatial variability distribution is considered uncertain because of the limited number of seepage test locations available and because the seepage test locations are clustered along the ESF and ECRB Cross-Drift, and thus do not provide full spatial coverage of all repository drift locations. In other words, there is uncertainty because the spatial variability distribution might be different if more test locations had been available or if test locations had been placed differently. In the TSPA seepage calculation, this uncertainty in spatial variability is the main source of uncertainty in the capillary-strength parameter. Two alternative approaches were evaluated for developing a distribution that adequately accounts for spatial variability uncertainty. The first approach applied an empirical method based on estimates of the standard error of the mean of the 10-point sample of capillary-strength values (SNL 2007, 6.6.2.3). The second approach used a statistical method based on maximum likelihood estimation to characterize the spatial variability and related uncertainty of the 10-point sample of capillary-strength values (SNL 2007, Section 6.6[a]). Results from the two approaches are very consistent and demonstrate that the assessment of spatial variability uncertainty of the capillary-strength parameter is appropriate. Uncertainty is accounted for in the TSPA seepage calculation by varying the spatially variable parameter values (sampled from the spatial variability distribution), with the magnitude of this variation sampled from the uncertainty distribution (SAR Sections 2.3.3.2.3.2, 2.3.3.2.3.6, and 2.3.3.4.1.1).

In summary, the injection tests and the test locations are representative of the repository rock conditions. The capillary-strength parameter calibrated from these injection tests is an effective process parameter that accounts for additional factors affecting seepage, and therefore is not strongly correlated to spatial variability between test locations. The spatial variability of the capillary-strength parameter and its uncertainty are adequately accounted for in the TSPA seepage calculation.

2. COMMITMENTS TO NRC

None.

3. DESCRIPTION OF PROPOSED LA CHANGE

None.

4. REFERENCES

BSC (Bechtel SAIC Company) 2004a. *Seepage Calibration Model and Seepage Testing Data*. MDL-NBS-HS-000004 REV 03. Las Vegas, Nevada: Bechtel SAIC Company. ACC: DOC.20040922.0003; DOC.20060808.0003.

BSC 2004b. *In Situ Field Testing of Processes*. ANL-NBS-HS-000005 REV 03. Las Vegas, Nevada: Bechtel SAIC Company. ACC: DOC.20041109.0001; DOC.20051010.0001; DOC.20060508.0001; DOC.20080724.0006.

BSC 2004c. *Drift Degradation Analysis*. ANL-EBS-MD-000027 REV 03. Las Vegas, Nevada: Bechtel SAIC Company. ACC: DOC.20040915.0010; DOC.20050419.0001; DOC.20051130.0002; DOC.20060731.0005; LLR.20080311.0066.

SNL (Sandia National Laboratories) 2007. *Abstraction of Drift Seepage*. MDL-NBS-HS-000019 REV 01 AD 01. Las Vegas, Nevada: Sandia National Laboratories. ACC: DOC.20070807.0001; DOC.20080813.0004; DOC.20081118.0049[a].

NOTE: [a]Provided as an enclosure to letter from Williams to Sulima dtd 02/17/2009. “Yucca Mountain – Request for Additional Information Re: License Application (Safety Analysis Report Section 2.1), Safety Evaluation Report Volume 3 – Postclosure Chapters 2.2.1.1 and 2.2.1.3.7 – Submittal of Department of Energy Reference Citations.”

RAI Volume 3, Chapter 2.2.1.3.6, Second Set, Number 4:

> Explain the basis for assuming uniform capillary strength at the scale of the drift seepage model domain. This information is needed to determine compliance with 10 CFR 63.114(a)(1,2).
>
> Basis: The rationale is not apparent for the uniformity assumption for the capillary strength parameter (BSC, 2004b, Section 5.4). The seepage model is populated with a heterogeneous permeability field, but a single value of capillary strength is derived. Observations of high and low flow zones from Alcove 6 (BSC, 2004a, Section 6.6), however, suggest variability on a short (~1m) length scale. In addition, estimates derived from theoretical and empirical considerations for fracture zones in Niches 3650 and 4788 suggest local variations are greater than three orders of magnitude (BSC, 2004a, Section 6.2.2.2, Table 6-9).

1. RESPONSE

The purpose of the seepage model for the total system performance assessment (TSPA) is to predict the incidence and rate of seepage at the scale of individual waste package locations. Therefore, both the seepage calibration model (SCM) (BSC 2004a) and the seepage model for performance assessment (SMPA) (BSC 2004b) simulate seepage at the drift scale. The capillary strength parameter ($1/\alpha$) cannot be directly measured. Its value is therefore determined by calibration (BSC 2004a, Sections 6.6.1.2 and 6.6.3.1). The uniform value at drift scale is appropriate because it is an effective parameter that incorporates both small scale variation and features not explicitly simulated (such as surface roughness, film flow, and drop detachment).

As pointed out in *Seepage Calibration Model and Seepage Testing Data* (BSC 2004a, Sections 6.6.1.2 and 8.4), the value of $1/\alpha$ depends upon the scale of discretization used in the mesh of the calibration model. It is therefore essential that $1/\alpha$ be used for predictive simulations in a model with the same scale of discretization. The SCM and the SMPA are both discretized at a scale of $0.1 \times 0.3 \times 0.1$ m, fulfilling that requirement.

Validation of the seepage models justifies the modeling approach and the input data, including the calibrated value of $1/\alpha$. Actual seepage observed in the south ramp of the Exploratory Studies Facility (ESF) in 2005 provides additional validation of the models (SNL 2007, Section 7.1[a]). The conceptual model for ambient seepage is described in SAR Section 2.3.3.2.1. Data and data uncertainty are described in SAR Section 2.3.3.2.2, and the modeling approach is described in SAR Section 2.3.3.2.3. The appropriateness of the modeling approach based on capillary diversion is justified in the response to RAI 3.2.2.1.3.6-2-005, Section 1.4. Small-scale estimates of $1/\alpha$ referenced in the RAI basis (BSC 2004c, Section 6.2.2.2, Table 6-9) are not appropriate for modeling seepage under repository conditions, as discussed below. Finally, the Alcove 6 observations referenced in the RAI basis have been incorporated in the developed framework.

The capillary strength parameter ($1/\alpha$) is not intended to characterize individual fractures; rather, it is an effective parameter appropriate for drift-scale simulation. The developed framework for simulating seepage in the TSPA-LA model uses a capillary strength parameter that is uniform at the drift scale and produces seepage predictions at the drift scale that are consistent with measured data. Spatial variability in capillary strength is captured in TSPA by sampling the effective capillary strength parameter on a waste package-by-waste package basis from the distributions shown in *Seepage Calibration Model and Seepage Testing Data* (BSC 2004a, Figure 6-32 and Table 6-8), and in *Total System Performance Assessment Model /Analysis for the License Application* (SNL 2008, Table 6.3.3-1). Individual seep flow rates are affected by the local percolation flux and the local flow diversion characteristics of the host rock. Flow diversion combines the effects of permeability, connectivity of the fracture network, and capillary retention. Spatial variability of permeability is incorporated explicitly and conditioned on spatially distributed measurements. Capillary strength is a calibrated parameter, developed as the target parameter in a nonlinear inversion (i.e., data-matching procedure). Capillary strength represents the ability of capillary forces in the fracture network to retain water in the fractures against pressure and gravitational forces. For a single fracture, capillary strength would be greater in smaller-aperture fractures; the calibrated value of $1/\alpha$ averages this property over all fractures intersecting the drift crown at a particular waste package location (with associated uncertainty and variability among locations). A calibration approach is necessary because all factors that could affect seepage (such as fracture connectivity and roughness, and the distribution of fracture apertures intersecting the drift crown) are not known at each waste package location, and can not be measured directly nor modeled explicitly. Capillary strength is thus an effective calibrated parameter. It is only weakly correlated with fracture permeability because many of the factors represented (e.g., connectivity) are not correlated or are not known at specific test locations.

The RAI basis suggests that the capillary strength parameter $1/\alpha$ should be represented explicitly in the seepage modeling framework (in addition to fracture permeability) as a spatially varying parameter at the small scale (e.g., 1 m). It is not necessary to vary $1/\alpha$ at small scale, because it is a calibrated effective parameter used at the drift scale to simulate seepage above individual waste packages. Use of a calibrated effective parameter ensures that the value captures the effect of small-scale features that are not explicitly simulated. Validation of the seepage calibration model (BSC 2004a, Section 7) shows that the use of a uniform $1/\alpha$ that is calibrated and used at drift scale produces conservative simulations of seepage.

Liquid release rates and seepage data for Niches 2 and 4 (also referred to as Niches 3650 and 4788) (BSC 2004c, Section 6.2.2.2, Table 6-9; cited in the RAI basis) were analyzed to produce estimates of capillary strength ($1/\alpha$) that vary on a scale of 0.3 m. However, this does not invalidate the use of a calibrated uniform value for a drift-scale model because the calibration averages small-scale variability to derive a value that is effective at drift scale. Note also that the capillary strength parameter estimates given in Table 6-9 are based on a definition of $1/\alpha$ (they were obtained by using the steady-state solution of Philip et al. 1989), which relies on a different characteristic equation to represent capillarity than used for the SCM and SMPA. The local capillary strength parameters in Table 6-9 were estimated using seepage data from short-term liquid-release tests in which very small amounts of water were injected. These seepage rates are therefore influenced by transient and storage effects, whereas the solution of Philip et al. (1989) assumes a steady-state flow field. These tests also probed rock volumes that were much smaller than the drift scale. Thus, while the resulting small-scale variability in capillary strength may appear consistent with the drift-scale variability used in TSPA (e.g., Niche 4, also known as Niche 4788), using a steady-state solution to evaluate transient seepage test data produced biased estimates of the seepage threshold with enhanced variability. The estimates of $1/\alpha$ shown in *In Situ Field Testing of Processes* (BSC 2004c, Table 6-9) were therefore not used in the seepage modeling framework for the TSPA. Data from Niche 2 tests were used for validation of the SCM, and data from some Niche 4 tests were used for calibration while others were used for validation (see BSC 2004a, Table 6-5).

This RAI basis statement also refers to observations of high- and low-flow zones from Alcove 6 (BSC 2004c, Section 6.6) as evidence for variability of fracture-network permeability on a short (~1 m) scale. Because both the SCM and the SMPA are discretized at a scale of $0.1 \times 0.3 \times 0.1$ m, with stochastically varying fracture-network permeability, the seepage modeling framework reproduces flow variability, with high- and low-flow zones, that is consistent with the observations from Alcove 6 (see for example BSC 2004a, Figure 6-21).

The calibrated capillary strength value ($1/\alpha$) is appropriate only for use with the same mathematical model and numerical discretization used in the inversion (BSC 2004b, Section 6.1; BSC 2004a, Section 6.6.3.1). Thus, the seepage model for performance assessment uses the same simulator and discretization as were used for seepage calibration. The effects of spatial variability and uncertainty associated with the calibration are propagated into the TSPA (SNL 2007, Section 6.6.2.3).

In summary, the use of a uniform drift-scale capillary strength parameter is appropriate because it is an effective parameter and the same discretization is used in both the SCM and the SMPA. The seepage modeling framework produces local seepage points and seepage variability due to local heterogeneity (see for example BSC 2004a, Figure 6-21), and seepage predictions on the drift scale that are consistent with measured data (BSC 2004a, Section 7). Note that although the SMPA appropriately simulates the process, the predicted values of seepage are conservative, as described in the response to RAI 3.2.2.1.3.6-2-005, Section 1.4, and in SAR Sections 2.3.3.2 and 2.3.3.3.

2. COMMITMENTS TO NRC

None.

3. DESCRIPTION OF PROPOSED LA CHANGE

None.

4. REFERENCES

BSC (Bechtel SAIC Company) 2004a. *Seepage Calibration Model and Seepage Testing Data*. MDL-NBS-HS-000004 REV 03. Las Vegas, Nevada: Bechtel SAIC Company. ACC: DOC.20040922.0003; DOC.20060808.0003.

BSC 2004b. *Seepage Model for PA Including Drift Collapse*. MDL-NBS-HS-000002 REV 03. Las Vegas, Nevada: Bechtel SAIC Company. ACC: DOC.20040922.0008; DOC.20051205.0001.

BSC 2004c. *In Situ Field Testing of Processes*. ANL-NBS-HS-000005 REV 03. Las Vegas, Nevada: Bechtel SAIC Company. ACC: DOC.20041109.0001; DOC.20051010.0001; DOC.20060508.0001; DOC.20080724.0006

Philip, J.R.; Knight, J.H.; and Waechter, R.T. 1989. "Unsaturated Seepage and Subterranean Holes: Conspectus, and Exclusion Problem for Circular Cylindrical Cavities." *Water Resources Research, 25,* (1), 16-28. Washington, D.C.: American Geophysical Union.

SNL (Sandia National Laboratories) 2007. *Abstraction of Drift Seepage*. MDL-NBS-HS-000019 REV 01 AD 01. Las Vegas, Nevada: Sandia National Laboratories. ACC: DOC.20070807.0001; DOC.20080813.0004; DOC.20081118.0049[a].

SNL 2008. *Total System Performance Assessment Model /Analysis for the License Application.* MDL-WIS-PA-000005 REV 00 AD 01. Las Vegas, Nevada: Sandia National Laboratories. ACC: DOC.20080312.0001; LLR.20080414.0037; LLR.20080507.0002; LLR.20080522.0113.

NOTE: [a]Provided as an enclosure to letter from Williams to Sulima dtd 02/17/2009. "Yucca Mountain – Request for Additional Information Re: License Application (Safety Analysis Report Section 2.1), Safety Evaluation Report Volume 3 – Postclosure Chapters 2.2.1.1 and 2.2.1.3.7 – Submittal of Department of Energy Reference Citations."

RAI Volume 3, Chapter 2.2.1.3.6, Second Set, Number 5:

> Explain why variability in seepage test results is best explained by capillary diversion, alternative conceptual models for the injection test observations are not valid, and seepage is not underestimated when using a model based on capillary diversion.
>
> Basis: SAR Section 2.3.3.2.3.1 describes a conceptualization of seepage based on capillary diversion at the drift wall. In situ seepage tests were performed along boreholes in the ECRB and ESF; some of the tests were selected for calibration of the seepage model. Considering all seepage tests, it often appears that injection rates vary abruptly from one packed interval to the next along the boreholes (BSC 2004, Sections 6.2. 6.6, and 6.11). Instead of capillary diversion, the abrupt changes possibly could be explained by variations in the nature of fractures that intersect the borehole. For example, the potential presence of horizontal fractures, small aperture subvertical fractures, or large aperture subvertical fractures may coincide with packed borehole sections where no water seeps, small amounts seep, or large amounts seep quickly. If the fracture network acted as a continuum on the scale of the injection testing, then the abrupt changes in injection and collected seepage back and forth along a borehole should not be expected.

1. RESPONSE

Seepage test results exhibit behavior consistent with capillary diversion, although other processes may be valid and are not excluded from the conceptual model. The key parameters of the seepage model include permeability, which is conditioned on measured data, and capillary strength, which is calibrated to seepage test results. The conditioned permeability fields allow for and include abrupt spatial changes in injection rates. The calibration results represent other diversion processes in addition to capillary diversion, and as implemented in the seepage abstraction for the total system performance assessment (TSPA) for the license application, they ensure that seepage is not underestimated.

1.1. CONCEPTUAL MODEL CONSIDERATIONS

The conceptual model (SAR Section 2.3.3.2.1) acknowledges the potential role of fractures and other structural features to determine spatially heterogeneous flow paths within the unsaturated zone. Supporting data and data uncertainty are described in SAR Section 2.3.3.2.2. Air-injection tests were performed in boreholes for hydrologic characterization, and seepage rate data were obtained primarily from liquid-release tests. The liquid-release tests metered water into borehole intervals and captured the resulting seepage into underlying drifts. These boreholes were drilled above niches excavated into the sidewalls of the main Exploratory Studies Facility (ESF) drift and the Enhanced Characterization of the Repository Block (ECRB) Cross-Drift. In addition, three test boreholes were drilled into the crown of the ECRB Cross-Drift (SAR Section 2.3.3.2.2.1).

The conceptual model that was used as the basis for liquid-release tests is summarized in six water balance components (SAR Section 2.3.3.2.2.1.4): (1) injected water; (2) seepage into the opening; (3) evaporation from the rock surface and the collection system; (4) storage in the formation between the injection point and the opening; (5) water that bypasses the opening through known and unknown geologic features; and (6) diversion around the opening because of the capillary-barrier effect. Component (5) of the conceptual model specifically included injected water that was diverted by structural features, such as fractures, between the point of injection and the underlying opening.

As described in SAR Section 2.3.3.2.2.1.4, attempts to directly measure the sum of components (5) and (6) in the water balance at Niche 5 (also known as Niche 1620) were unsuccessful. However, the other components in the water balance were measured or directly estimated for many liquid release tests, and the calibrated seepage model conceptual approach relies on a water balance that combines components (5) and (6), which is appropriate for modeling seepage into the drift opening (see response to RAI 3.2.2.1.3.6-2-004).

1.2. HETEROGENEITY

The effects of rock mass heterogeneity were investigated in seepage testing, and addressed in seepage modeling. Air-injection testing included many tests conducted sequentially in one-foot borehole intervals to measure small-scale permeability variations (SAR Section 2.3.3.2.2.1.2), including abrupt spatial changes. These permeability variations are incorporated in seepage simulations as heterogeneous, spatially correlated permeability fields conditioned on the statistics of variability of the measurements (SAR Section 2.3.3.2.3.6.2). Numerous liquid-release tests were also conducted, in Niches 2, 3, 4, and 5 (also known as Niches 3650, 3107, 4788, and 1620) and in the systematic testing area in the ECRB Cross-Drift. Seepage rate data from 22 liquid-release tests conducted in Niches 3, 4, and 5, and in three boreholes drilled from the ECRB Cross-Drift, were used to calibrate the seepage calibration model, to estimate the capillary strength parameter. Most of the remaining test data (an additional 59 tests) were simulated with the calibrated seepage model (SAR Section 2.3.3.2.3.3) to evaluate how the model represents rock mass heterogeneity. Uncertainty was propagated into the TSPA as probability distributions that characterize spatial variability and uncertainty in the capillary strength parameter (SAR Section 2.3.3.2.3.6.1).

The liquid-release test design and the construction of the models were designed to appropriately represent seepage into emplacement drift intervals corresponding to the approximate length of a waste package (SAR Section 2.3.3.2.3.2). Numerical simulations supporting the seepage model used a stochastic continuum for bulk permeability, with the capability to incorporate strong heterogeneity leading to abrupt changes in flow rates (SAR Section 2.3.3.2.3.2). Variability in hydraulic connectivity of the fracture network was represented using multiple realizations of the permeability field, in which permeability was discretized on a cell-by-cell basis (SAR Section 2.3.3.2.3.6.2). In the seepage abstraction used for the TSPA, the key uncertain rock parameters (rock permeability and capillary strength; SAR Section 2.3.3.2.3.6) are re-sampled for each waste package location, allowing similarly abrupt changes in estimated seepage rates. Thus, using a continuum approach in seepage modeling does not imply that calculated injection and seepage rates are uniform from grid cell to grid cell, or that estimated seepage varies smoothly among waste package locations.

1.3. DISTINGUISHING AMONG CONCEPTUAL MODELS

The liquid-release tests were designed to help select the most appropriate conceptual models. Diversion through subhorizontal fractures or other structural features between the point of injection and the underlying opening was identified as a possibility. Some tests were determined to be inappropriate for investigating seepage. For example, because of the large (approximately 20-m) distance between the release and collection points in the Alcove 8-Niche 3 test, some of the released water may have bypassed the niche and seepage collection system due to structural features (SAR Section 2.3.3.2.2.1.5). The Alcove 8-Niche 3 test was developed for tracer transport studies, and provided limited value to the seepage model because interpretation of near-field diversion processes could have been influenced by flow heterogeneity in the far field. Accordingly, the results were not used for seepage parameter estimation (SAR Section 2.3.3.2.3.4.3).

To limit the effects of structural diversion on liquid-release testing, the injection holes were located close to the underlying excavated openings. In addition, the seepage tests were designed to provide information about the seepage process on the scale of an emplacement drift (SAR Section 2.3.3.2.2.1.6). This was accomplished by excavating the test niches to nearly the same cross-section (a nominal width of 4 m; BSC 2004b, Figures 6-4 and 6-6) as the repository emplacement drifts (a nominal width of 5.5 m; BSC 2004a, Section 6.3.3.3). The ECRB Cross-Drift, where three additional test boreholes were drilled, has a nominal width of 5 m (BSC 2004a, Section 6.3.3.3).

The distance between the release and collection points in the niche tests used for seepage parameter estimation (Niches 2 through 5) ranged from about 0.4 to 1.4 m. These distances were estimated from the niche cross sections in Figures 6-4 and 6-35 of *In Situ Field Testing of Processes* (BSC 2004b). Niche 4 is an 8.2-m-long drift located in an intensely fractured zone (BSC 2004a), Section 6.5.1). The travel distance in the Niche 4 test ranged from about 1.1 to 1.4 m and significant bypassing due to structural features is unlikely over such a small distance (SAR Section 2.3.3.2.2.1.1).

The release and seepage rates observed in a high release-rate test (0.04 gal/s or about 9,100 ml/min) in Niche 4 are shown in SAR Figure 2.3.3-9. In this example, because of the high release rate, a near-steady seepage rate developed that was approximately 60% of the release rate. This indicates that the diversion rate was approximately 40% of the release rate, even at this highly elevated release rate and short travel distance. In lower release-rate tests, the diverted fraction was generally much larger, and the proportion of seepage was generally much smaller. The release rates in tests used for model calibration ranged from 0.5 to 44.5 ml/min (BSC 2004a, Table 6-5). These rates were smaller than in the high release-rate test, to maintain representative, unsaturated flow in the fractures.

This response evaluates alternative approaches to interpreting the liquid-release tests, based on whether structural features such as fractures: (1) divert all percolating water, allowing none to seep; (2) divert part of the percolating water allowing small amounts to seep; or (3) divert none of the percolating water, allowing large amounts to seep quickly. If all water in the liquid-release tests were diverted by subhorizontal fractures, there would be no seepage. This is possible, but a lack of seepage rarely occurred in liquid-release tests where the total released volume was considered sufficient to overcome water storage effects. Test events used for the calibration and validation of the seepage calibration model are described in Table 6-5 and Section 6.5.3 of *Seepage Calibration Model and Seepage Testing Data* (BSC 2004a). Of the 26 borehole intervals used for calibration and validation, only one test interval (test events 72 to 76 in borehole SYBT-ECRB-LA#3, Zone 2) likely had sufficient liquid release volume and rate but exhibited no seepage. This lack of seepage could have resulted from structural diversion, capillary diversion, or a combination of the two.

Test results demonstrate that while diversion by sub-horizontal fractures is possible, it is unlikely to be the only seepage-exclusion effect. The onset of seepage is almost always observed as liquid release rates are increased. Consider the following example. Borehole SYBT-ECRB-LA#3 is one of three 15^{o} upward-inclined liquid release holes drilled into the crown of the ECRB Cross-Drift (BSC 2004a, Section 6.5.1). The second zone in this borehole is located between 10.4 and 12.2 m from the collar. The average distance of SYBT-ECRB-LA#3 Zone 2 above the crown of the underlying drift is 2.9 m. This distance is approximately three times greater than the typical travel distances in the niche tests, increasing the possibility of structural diversion. Other test intervals where no seepage occurred were either: (a) too tight for water to be released into the formation (test event 77 in borehole SYBT-ECRB-LA#3, Zone 3); (b) had release volumes that were too small (all test events in Niche 2; approximately one liter per test event); (c) had release rates that were too small (test events 1-3 in Niche 3; maximum release rate of 2 ml/min); or (d) had leaking packers (test events 79 to 80 in Niche 5). Except for the tests with packer failures in Niche 5, all tests with injection rates greater than 100 ml/min exhibited seepage (BSC 2004a, Table 6-5 and Section 6.5.3).

Liquid-release test results generally exhibited progressively less diversion as the liquid-release rate was increased. This is not well represented by a conceptual alternative in which most of the water was diverted by large aperture, subhorizontal fractures and a small amount flowed through small aperture, subvertical fractures and appeared as seepage. For this alternative, the seepage flux would be relatively insensitive to the release rate because most of the released water would be diverted by the large aperture fractures, and there would be no significant additional barrier to seepage at the drift wall. With capillary diversion, however, the fraction of injected water that seeps is expected to be initially near zero, and to increase with increasing liquid release rates (SAR Section 2.3.3.2.3.4.1). This occurs because the highest capillary pressure occurs in the narrowest fractures, and these are the fractures that saturate first, reducing the overall capillary pressure as the liquid release rate increases.

Liquid-release tests did not generally exhibit seepage rates that approached the respective release rates, which is inconsistent with the conceptual alternative in which most of the released water flowed into the drift through large aperture subvertical fractures. For this conceptual alternative, steady seepage rates would be essentially the same as the liquid release rates. The near-steady seepage rates from the tests that were used for model calibration were generally less than half (and often much less than half) of the liquid release rates (BSC 2004a, Section 6.6.3.2 and Figures 6-19, 6-22, 6-23, 6-24, 6-29, and 6-31).

An alternative conceptual model that infers seepage rates from precipitates in lithophysal cavities is discussed in SAR Section 2.3.3.2.3.7.4. This model considered calcite precipitation mechanisms and assumed that water entered the lithophysal cavities as seepage. The analysis demonstrated that not all lithophysal cavities have calcite deposits, and that estimates of the seepage flux derived from the calcite deposits are significantly smaller than estimates of seepage into repository drifts as predicted by TSPA using the seepage model. Although these results corroborated the concept of seepage being less than the percolation flux, this conceptual model was rejected because it could significantly underestimate seepage. This alternative conceptual model is discussed in the response to RAI 3.2.2.1.3.6-2-007.

Stress redistribution during drift excavation leads to local opening or partial closing of fractures and, potentially, the creation of new fractures. The ambient seepage models use excavation-disturbed rock properties to simulate seepage, capturing this effect (SAR Section 2.3.3.2.1.3). If flow diversion through fractures associated with drift excavation were significant during seepage testing, the same effect would affect water diversion during the performance period.

1.4. APPROPRIATENESS OF SEEPAGE ESTIMATES

The seepage model used for TSPA is based on calibrated effective capillary strength and permeability parameters that realistically incorporate variability and uncertainty (SAR Section 2.3.3.6). Conservative elements have been incorporated to ensure that predicted seepage rates are generally higher than actual rates. Key conservatisms are used to represent conditions that deviate from ambient conditions, so that seepage is not underestimated in situations where uncertainties are greater. For example, although simulations show that seepage will be reduced at elevated temperature conditions during drift cooldown, the predicted seepage rate is set equal to the higher ambient rate as soon as drift wall temperatures drop below 100°C (SAR Section 2.3.3.3.4). Also, the increased uncertainty in seepage simulation results for degraded drifts is accounted for by using upper bound estimates based on worst case drift profiles to represent conditions after collapse (SAR Section 2.3.3.2.4.2.2). Evidence that seepage is not underestimated under ambient conditions is provided by model validation runs and by simulating *in situ* observations of natural seepage in the ESF South Ramp. Together, these demonstrate that use of a conservative model based on uncertainty distributions of percolation flux data, effective permeability, and effective capillary strength does not underestimate seepage.

Model validation runs were conducted in which seepage rates for liquid-release tests conducted in Niche 3 and not used in model development were estimated using the seepage calibration model. The results show that the seepage calibration model overestimates seepage, for the tests at low injection rates where little or no seepage is predicted (corresponding to the top four plots in SAR Figure 2.3.3-18). Results for seepage tests with relatively high injection rates (corresponding to the bottom four plots in SAR Figure 2.3.3-18) show that measured seepage is generally within the 95% uncertainty band, and less than the mean simulated seepage except for the tests conducted on October 11, 1999 (the bottom right plot in SAR Figure 2.3.3-18), in which the measured seepage falls close to the upper bound of the uncertainty band and is more than the simulated seepage. The injection rates used in these tests were significantly greater than the background percolation flux, to achieve a measurable seepage.

Seepage calculations for the ESF South Ramp seepage event are summarized in SAR Section 2.3.3.4.3. Precipitation events in the fall of 2004 and winter of 2005 resulted in wet spots on the crown, ribs, and invert of the ESF South Ramp. A qualitative validation study examined whether the approach used to predict seepage into emplacement drifts yields results consistent with the observed South Ramp seepage. Assuming reasonable probability distributions for fracture-continuum permeability, capillary strength, and local percolation flux, the modeling approach estimated that seepage would occur along 37% of the ESF South Ramp section where the Paintbrush Tuff nonwelded unit is not present, compared with the observation that approximately 13% of this section of the ESF South Ramp exhibited wet spots in February 2005. Thus, the seepage simulations yielded results that conservatively overestimate, but are generally consistent with, observations made in the South Ramp.

1.5. SUMMARY

Spatial heterogeneity in fracture permeability and seepage rates has been incorporated into the test design and seepage model. The conceptual model for seepage includes capillary diversion and diversion by structural features such as fractures. The capillary strength parameter determined by model calibration is an effective parameter that captures all flow diversion effects, including the potential for water to be diverted around a drift by structural features. Both components in the seepage water balance results have the same effect on repository performance, reducing seepage. Appropriate, conservative estimates for flow diversion are provided by the seepage abstraction used in the TSPA. The possibility that flow was diverted around the test drifts by structural features such as fractures is therefore included in the seepage model. Model validation demonstrates that predicted seepage rates exceed measured rates in almost all test cases, and are within uncertainty bands in all cases.

2. COMMITMENTS TO NRC

None.

3. DESCRIPTION OF PROPOSED LA CHANGE

None.

4. REFERENCES

BSC (Bechtel SAIC Company) 2004a. *Seepage Calibration Model and Seepage Testing Data.* MDL-NBS-HS-000004 REV 03. Las Vegas, Nevada: Bechtel SAIC Company. ACC: DOC.20040922.0003; DOC.20060808.0003.

BSC 2004b. *In Situ Field Testing of Processes.* ANL-NBS-HS-000005 REV 03. Las Vegas, Nevada: Bechtel SAIC Company. ACC: DOC.20041109.0001; DOC.20051010.0001; DOC.20060508.0001; DOC.20080724.0006.

RAI Volume 3, Chapter 2.2.1.3.6, Second Set, Number 6:

> Justify the use of a seepage threshold below which no seepage occurs despite a percolation flux. Explain the basis for the value selected for the seepage threshold. Explain how seepage fraction and release of radionuclides to the unsaturated zone are affected by the value selected for the seepage threshold. This information is needed to determine compliance with 10 CFR 63.114(a)(1,2,3,7).
>
> Basis: BSC (2007) states that values below 0.1 kg/yr per waste package are mainly a result of the interpolation procedure. No further discussion or basis could be found for this value.
>
> It is not clear how changes to the seepage threshold value would affect estimates of seepage fraction. The seepage fraction (SAR Section 2.3.3.2.1) depends on selection of a value for the seepage threshold. Furthermore, selection in TSPA of advective or diffusive algorithms for radionuclide release out of the waste package and through the invert depends, in part, on the seepage threshold value. The basis is not transparent for the threshold value for which the seepage model flux result is small enough to warrant setting the table entry to zero.

1. RESPONSE

1.1 IMPLEMENTATION OF THE TSPA SEEPAGE MODEL

The mean and standard deviation for the distribution of seepage rates at a waste package location, corresponding to a given combination of capillary strength, permeability, and percolation flux, are estimated by interpolation from the seepage lookup tables developed in *Seepage Model for PA Including Drift Collapse* (BSC 2004) and extended to cover a wider percolation flux range in *Abstraction of Drift Seepage* (SNL 2007, Section 6.1[a]). The extended lookup tables provide computed mean and standard deviation for the distribution seepage rates for percolation flux ranging from 0.01 to 5,000 mm/yr (32 values), log permeability ranging from −10 to −14 (17 values), and capillary strength ranging from 100 to 1,000 Pa (10 values). Thus, the extended seepage lookup tables have 32 × 17 × 10 = 5,440 seepage values representing intact drifts, and another 5,440 values for collapsed drifts. In these extended lookup tables, values of mean seepage rate less than 0.1 kg/yr per waste package (a seepage cut-off value, referred to as threshold seepage, as distinguished from the seepage threshold percolation flux) and greater than zero are rare (SNL 2007, Section 6.8). For the intact drifts only 41 (0.75%) out of 5,440 simulated values in the extended seepage lookup table are between zero and 0.1 kg/yr per waste package, and 1,472 (27.1%) have zero seepage. For the collapsed drift scenario, the extended seepage lookup table has 53 (0.97%) values with seepage rate between zero and 0.1 kg/yr per waste package, and 1,019 (18.7%) values with zero seepage. The distribution of calculated mean seepage values in these extended lookup tables provides the basis for interpolation of seepage over the range of percolation flux, permeability, and capillary strength represented in the total system performance assessment (TSPA) model. This distribution of points in the lookup tables provides sufficient resolution to define the transition from zero to non-zero seepage needed for the interpolation. In the demonstration of a probabilistic estimate of the number of waste package locations with drift seepage (SNL 2007, Section 6.8), and in the TSPA calculation of seepage fraction (SNL 2008, Section 6.3.3.1.3), locations with an interpolated seepage rate cut-off value of less than 0.1 kg/yr per waste package are counted as locations where seepage does not occur.

1.2 EFFECT OF ZERO THRESHOLD SEEPAGE ON SEEPAGE FRACTION

To obtain the mean of the distribution of seepage rate corresponding to permeability, capillary strength, and local percolation flux (i.e., percolation flux after adjustment by the local flow focusing factor) at any waste package location in the drift, a linear interpolation of the results (mean seepage rate and related standard deviation) of the extended seepage lookup table is performed and the resulting mean seepage rate adjusted for seepage uncertainty (SNL 2007, Figure 6-1[a] and Section 6.4[a]). The seepage rate at a given location is then sampled from a normal distribution described by the mean and standard deviation of seepage rates. For parameter combinations that produce near-zero seepage rate, this interpolation, adjustment for mean seepage rate uncertainty, and sampling may yield very small values of seepage rate (as low as 10^{-10} kg/yr per waste package). Thus, if no threshold seepage value (or a zero value) is used, many small values of interpolated seepage rate would be counted as seeping locations and the seepage fraction would increase.

The sensitivity of seepage fraction to the threshold seepage value is demonstrated by a probabilistic analysis of seepage, conducted using the seepage abstraction for the TSPA, and 10,000 random parameter samples (SNL 2007, Sections 6.8 and 6.4[a]). This analysis uses the same distributions of percolation flux, permeability, and capillary strength as those used to estimate seepage in the TSPA (SNL 2008, Section 6.3.3.1.3). As documented for the TSPA, the probabilistic analysis used a threshold seepage value of 0.1 kg/yr per waste package. For this RAI response, the seepage fraction is recalculated with the seepage threshold set to zero. The results are compared with respect to the mean seepage rate, the mean seepage percentage, and the seepage fraction (SNL 2007, Section 6.1.3), during the present-day, the monsoon, and the glacial-transition climates (Tables 1 and 2; similar to SNL 2007, Tables 6-6[a] and 6-7[a]).

For intact drifts (Table 1), using the percolation flux based on the present-day 10th percentile infiltration map increases the seepage fraction from 7.6% with 0.1 kg/yr per waste package threshold seepage to 11.2% with threshold seepage set to zero. The seepage fraction increases from 13.4% to 17.3% for the monsoon climate, and from 17.0% to 20.6% for the glacial-transition climate. The use of a zero threshold seepage value does not significantly change the amount of seeping water, or the seepage percentage. On average over all waste packages, the amount of seeping water is approximately 1.2, 4.6, and 14.4 kg/yr per waste package for the three pre-10,000-year climate stages, respectively. This translates to mean seepage percentages of 1.1%, 2.2%, and 4.7% for the three pre-10,000-year climate stages respectively. In other words, during the present-day climate, an average of about 99% of the percolation flux would be diverted around intact drifts in the Tptpll (Topopah Spring Tuff lower lithophysal) unit, for example. For the wetter climate stages of the monsoon and the glacial-transition periods, the mean percentage of diverted flux would be smaller, but still at about 98% and 95%, respectively (Table 1).

For the 30th percentile infiltration scenario, the seepage fraction increases from 16.7% to 20.4% for the present-day climate, from 22.8% to 26.2% during the monsoon period, and from 29.5% to 32.7% during the glacial-transition climate. For the 90th percentile infiltration scenario, seepage fraction increases from a high of 52.6% to 54.3% during the monsoon climate (i.e., more than half of all waste packages experience some amount of seepage). For the post-10,000-year case, the largest seepage fraction increases from 45.2% to 47.3%. Table 2 shows the results for the collapsed drift case, which are similar to the results for the intact drift case. The results show that using threshold seepage of 0.1 kg/yr per waste package or zero kg/yr per waste package has a very small effect on seepage fraction (approximately 1% to 5% change), for the longer duration monsoon and glacial-transition climate states that dominate the period when seepage into drifts is most likely. Changes in seepage fraction of this magnitude produce negligible effects on repository performance (SNL 2008, Section 7.3.1.5[a]). In the TSPA, the seepage fraction for each percolation subregion is defined as a constant parameter based on the percolation flux at the end of the simulation period (either 10,000 years or 1,000,000 years) (SNL 2008, Section 8.3.3.1.1[a], and Tables 8.3-2[a] and 8.3-3[a]).

Table 1. Summary Statistics for Probabilistic Seepage Evaluation (Intact Drifts)

	Mean Seepage Rate (kg/yr/WP)	Mean Seepage Percentage (%)	Seepage Fraction (%) 0.1 kg/yr/WP Threshold	Seepage Fraction (%) 0.0 kg/yr/WP Threshold	Change in Seepage Fraction
10 Percentile Infiltration Scenario					
Present-Day	1.2	1.1	7.6	11.2	3.6
Monsoon	4.6	2.2	13.4	17.3	3.9
Glacial-Transition	14.4	4.7	17.0	20.6	3.6
30 Percentile Infiltration Scenario					
	Mean Seepage Rate (kg/yr/WP)	**Mean Seepage Percentage (%)**	**Seepage Fraction (%) 0.1 kg/yr/WP Threshold**	**Seepage Fraction (%) 0.0 kg/yr/WP Threshold**	**Change in Seepage Fraction**
Present-Day	8.1	3.0	16.7	20.4	3.7
Monsoon	20.5	4.9	22.8	26.2	3.4
Glacial-Transition	54.0	8.0	29.5	32.7	3.2
50 Percentile Infiltration Scenario					
	Mean Seepage Rate (kg/yr/WP)	**Mean Seepage Percentage (%)**	**Seepage Fraction (%) 0.1 kg/yr/WP Threshold**	**Seepage Fraction (%) 0.0 kg/yr/WP Threshold**	**Change in Seepage Fraction**
Present-Day	16.5	4.3	21.6	25.0	3.4
Monsoon	30.4	6.0	25.4	28.6	3.2
Glacial-Transition	98.4	10.7	33.9	36.8	2.9
90 Percentile Infiltration Scenario					
	Mean Seepage Rate (kg/yr/WP)	**Mean Seepage Percentage (%)**	**Seepage Fraction (%) 0.1 kg/yr/WP Threshold**	**Seepage Fraction (%) 0.0 kg/yr/WP Threshold**	**Change in Seepage Fraction**
Present-Day	82.9	9.3	34.9	37.7	2.8
Monsoon	470.8	19.5	52.6	54.3	1.7
Glacial-Transition	297.1	16.5	46.1	48.4	2.3
Post-10,000-Years					
	Mean Seepage Rate (kg/yr/WP)	**Mean Seepage Percentage (%)**	**Seepage Fraction (%) 0.1 kg/yr/WP Threshold**	**Seepage Fraction (%) 0.0 kg/yr/WP Threshold**	**Change in Seepage Fraction**
Infiltration Map 1	35.2	6.3	27.3	30.6	3.3
Infiltration Map 2	119.8	11.7	35.5	38.3	2.8
Infiltration Map 3	178.3	13.4	40.9	43.4	2.5
Infiltration Map 4	237.2	14.7	45.2	47.3	2.1

NOTES: WP = waste package.

The seepage statistics presented in this table correspond to those presented in *Abstraction of Drift Seepage* (SNL 2007, Table 6-6[a]), and are for illustrative purposes. The seepage fractions used in TSPA are based on the same abstraction model, but with differences imposed by implementation in the system model (SNL 2008, Section 6.3.3.1.3).

Table 2. Summary Statistics for Probabilistic Seepage Evaluation (Collapsed Drifts)

10 Percentile Infiltration Scenario					
	Mean Seepage Rate (kg/yr/WP)	**Mean Seepage Percentage (%)**	**Seepage Fraction (%) 0.1 kg/yr/WP Threshold**	**Seepage Fraction (%) 0.0 kg/yr/WP Threshold**	**Change in Seepage Fraction**
Present-Day	9.9	4.7	26.3	32.0	5.7
Monsoon	32.2	7.9	35.9	40.8	4.9
Glacial-Transition	78.3	12.8	39.6	43.9	4.3
30 Percentile Infiltration Scenario					
	Mean Seepage Rate (kg/yr/WP)	**Mean Seepage Percentage (%)**	**Seepage Fraction (%) 0.1 kg/yr/WP Threshold**	**Seepage Fraction (%) 0.0 kg/yr/WP Threshold**	**Change in Seepage Fraction**
Present-Day	51.6	9.7	40.1	44.6	4.5
Monsoon	114.0	13.6	47.7	51.5	3.8
Glacial-Transition	257.5	19.1	55.2	57.9	2.7
50 Percentile Infiltration Scenario					
	Mean Seepage Rate (kg/yr/WP)	**Mean Seepage Percentage (%)**	**Seepage Fraction (%) 0.1 kg/yr/WP Threshold**	**Seepage Fraction (%) 0.0 kg/yr/WP Threshold**	**Change in Seepage Fraction**
Present-Day	95.4	12.5	46.1	49.9	3.8
Monsoon	158.1	15.7	50.6	53.9	3.3
Glacial-Transition	429.6	23.3	58.9	61.4	2.5
90 Percentile Infiltration Scenario					
	Mean Seepage Rate (kg/yr/WP)	**Mean Seepage Percentage (%)**	**Seepage Fraction (%) 0.1 kg/yr/WP Threshold**	**Seepage Fraction (%) 0.0 kg/yr/WP Threshold**	**Change in Seepage Fraction**
Present-Day	381.4	21.5	60.9	63.4	2.5
Monsoon	1709.9	35.4	75.6	76.6	1.0
Glacial-Transition	1137.0	31.6	70.4	72.1	1.7
Post-10,000-Years					
	Mean Seepage Rate (kg/yr/WP)	**Mean Seepage Percentage (%)**	**Seepage Fraction (%) 0.1 kg/yr/WP Threshold**	**Seepage Fraction (%) 0.0 kg/yr/WP Threshold**	**Change in Seepage Fraction**
Infiltration Map 1	183.0	16.3	52.9	56.1	3.2
Infiltration Map 2	509.4	24.8	60.6	63.2	2.6
Infiltration Map 3	731.2	27.4	66.2	68.2	2.0
Infiltration Map 4	944.7	29.4	70.3	71.9	1.6

NOTES: WP = waste package.

The seepage statistics presented in this table correspond to those presented in *Abstraction of Drift Seepage* (SNL 2007, Table 6-7[a]), and are for illustrative purposes. The seepage fractions used in TSPA are based on the same abstraction model, but with differences imposed by implementation in the system model (SNL 2008, Section 6.3.3.1.3).

1.3 IMPACT OF THRESHOLD SEEPAGE ON REPOSITORY PERFORMANCE

A detailed discussion of the uncertainty in TSPA seepage fraction for the different modeling cases, including 10,000-year and 1,000,000-year cases, is presented in response to RAI 3.2.2.1.3.6-010 (Sections 1.2 to 1.5; Tables 4 through 10). The analysis shows that a wide range of values for the seepage fraction is used in the TSPA. As demonstrated in that response (RAI 3.2.2.1.3.6-010, Section 1.6, Figure 2) the example calculation of drift seepage (SAR Section 2.3.3.4.2; SNL 2007, Section 6.4[a]) that is used in this response (Tables 1 and 2) is consistent with the implementation of seepage in the TSPA.

The sensitivity of repository performance to uncertainty in the seepage fraction is discussed in the response to RAI 3.2.2.1.3.6-006 (Section 1.4.2 and Figure 1). The analysis shows that the total expected dose is insensitive to changes in seepage fraction. Therefore, the use of a zero value for threshold seepage (instead of the 0.1 kg/yr per waste package value used for TSPA), which would result in a 1% to 5% increase in seepage fraction and but no significant change in the total volume of seepage would have an insignificant effect on repository performance.

1.4 CONCLUSION

In conclusion, setting the threshold seepage at 0.1 kg/yr per waste package is a reasonable approximation for estimating the number of waste package locations with seeping conditions. Setting this threshold to zero would slightly increase the seepage fraction, but has no significant impact on estimates of repository performance.

2. COMMITMENTS TO NRC

None.

3. DESCRIPTION OF PROPOSED LA CHANGE

None.

4. REFERENCES

BSC (Bechtel SAIC Company) 2004. *Seepage Model for PA Including Drift Collapse.* MDL-NBS-HS-000002 REV 03. Las Vegas, Nevada: Bechtel SAIC Company. ACC: DOC.20040922.0008; DOC.20051205.0001.

SNL (Sandia National Laboratories) 2007. *Abstraction of Drift Seepage.* MDL-NBS-HS-000019 REV 01 AD 01. Las Vegas, Nevada: Sandia National Laboratories. ACC: DOC.20070807.0001; DOC.20080813.0004; DOC.20081118.0049[a].

SNL 2008. *Total System Performance Assessment Model/Analysis for the License Application.* MDL-WIS-PA-000005 REV 00 AD 01. Las Vegas, Nevada: Sandia National Laboratories. ACC: DOC.20080312.0001; LLR.20080414.0037; LLR.20080507.0002; LLR.20080522.0113; DOC.20080724.0005; DOC.20090106.0001[a].

NOTE: [a]Provided as an enclosure to letter from Williams to Sulima dtd 02/17/2009. "Yucca Mountain – Request for Additional Information Re: License Application (Safety Analysis Report Section 2.1), Safety Evaluation Report Volume 3 – Postclosure Chapters 2.2.1.1 and 2.2.1.3.7 – Submittal of Department of Energy Reference Citations."

RAI Volume 3, Chapter 2.2.1.3.6, Second Set, Number 7:

Explain the apparent discrepancy of the conceptualizations for water entering lithophysae between the (i) seepage model conceptualization of capillary diversion around openings such as drifts, and (ii) use of the laminar layers of mineralization in lithophysae for validation of percolation rates. This information is needed to evaluate compliance with 10 CFR 63.114 (a,b,c,g).

Basis: Seepage into lithophysae would not be expected to occur based on the importance of capillary diversion in the seepage model conceptualization. Lithophysae are small openings compared to drift openings; the former generally being more than an order of magnitude smaller than drift openings. The size and shape of an opening in porous media strongly affects the capillary diversion around that opening. Philip, et al. (1989), which is cited in BSC (2007), showed that spherical is the optimal shape for capillary diversion of water around openings. Consistent with Phillips et al. (1989), small, spherical openings more readily divert water percolating water as compared to large, cylindrical openings. SAR Section 2.3.3.2.3.7.4 describes inferences for seepage from precipitates in lithophysal cavities.

However, DOE suggests that percolation estimates are supported by isotopic dating of laminar layers within secondary mineralization found in fractures and cavities (SAR Section 2.3.2.3.4.4 and SNL, 2007 Section 7.7). This implies percolating water readily entered lithophysae, such that total percolation rates would be reflected in the secondary mineralization.

1. RESPONSE

Seepage, as it applies to modeling in support of the total system performance assessment (TSPA) refers to dripping liquid water into the drift opening; this definition of seepage (SNL, 2008a, Section 6.3.3.1) differentiates between dripping conditions and film flow (SAR, Section 2.3.2.4.2.1.6). Slow, continuous mineral precipitation within lithophysal cavities indicates that percolating water enters such cavities. The mechanism for water entry into the lithophysal cavities is not dripping (i.e., seepage), but rather, is film flow. Thus, there is not a discrepancy between the conceptualizations for water entering lithophysae between the (i) seepage model conceptualization of capillary diversion around openings such as drifts, and (ii) use of the laminar layers of mineralization in lithophysae for validation of percolation rates.

1.1 DESCRIPTION OF SEEPAGE IN TSPA MODELING

Drift seepage refers to the dripping of liquid water from the unsaturated zone above the repository into waste emplacement drifts (SNL 2008a, Section 6.3.3.1). For modeling purposes, only water that drips is defined as seepage to be explicitly modeled by the seepage model for performance assessment (SNL 2007b, Section 6.3.1). Water traveling down the drift walls as a film cannot contact the drip shield or waste package, and is assumed to be resorbed by the sloping wall of the drift prior to reaching the invert, because drift wall saturations decrease while progressing downwards along the wall (BSC 2005, Section 6.2.2). Hence, water flowing as a film down the drift wall is not a component of seepage (as defined here and in the response to RAI 3.2.2.1.3.6-2-008) and does not contribute to flux through the invert.

Water flow in the rock adjacent to the emplacement drifts occurs by a film flow process (BSC 2004a, Section 6.2.2). This differs from the traditional view of a flow in a capillary network where the wetting phase exclusively occupies capillaries with apertures smaller than some level defined by the capillary pressure. As a result, film flow in rock adjacent to the drift crown could allow water to enter a waste emplacement drift at nonzero capillary pressure. In addition, collection of film flow water on the local minima of surface roughness features along the crown of the drift could result in dripping (seepage). The effects of film flow are accounted for in the seepage model by use of an effective capillary strength parameter ($1/\alpha$), as also described in the context of features, events, and processes (FEPs) under included FEP 2.2.07.18.0A, Film Flow into the Repository (SNL 2008b). The effective capillary strength parameter implicitly incorporates the effects of film flow processes because it is derived by calibration against measured seepage test data which reflect film flow processes (BSC 2004b, Section 6.6.3.1 and Table 6-8). Estimates of seepage in both *Seepage Model for PA Including Drift Collapse* (BSC 2004a, Section 6.3) and *Abstraction of Drift Seepage* (SNL 2007b, Section 6.4.1.1) use the range of capillary-strength parameter values developed by the seepage calibration model, and hence incorporate the effects of film flow.

1.2 MINERAL PRECIPITATION IN LITHOPHYSAL CAVITIES

The calcite and opal coatings on fractures and within lithophysae are the main laminar mineralization coatings found in lithophysae and are common throughout the Topopah Spring welded hydrogeologic unit, and were each deposited by similar mechanisms. Although high-angle fractures only host thin (<1 cm) coatings of secondary minerals, low-angle fractures and, in particular, lithophysal cavities are the sites of thicker coatings (Paces et al. 2001). On a micro-scale, the calcite and opal are layered; dating and elemental analysis of these layers reveals that the thicker coatings formed at fairly constant rates and that climate-related changes in elemental composition are present. These results indicate that changes in mean annual precipitation and temperature and changes between wetter and drier climate states during the past 300,000 years, which should have produced large variations in near-surface infiltration, did not produce similarly large variations in fluid flux into lithophysae at the proposed repository horizon (Whelan et al. 2006). Calculations of the water volumes required to deposit calcite were based on a statistical representation of coating volumes (Marshall et al. 2003).

The calcite and opal coatings within the lithophysal cavities do not contain evidence, such as stalactites or stalagmites, of dripping water (BSC 2004a, Section 6.4.3). The distribution and texture of secondary minerals within fractures and cavities in the host rock are consistent with formation from thin water films that are unevenly distributed across a fracture surface or are drawn up the faces of growing crystals by surface tension (Whelan et al. 2002, Section 6). Examples of speleothems that have been attributed to water films are cited by Whelan et al. (2002, Section 5.2). Whelan et al. (2005, Section 2.3) discuss additional evidence for film flow as a mechanism to explain observed secondary mineral textures; they also show the results of laboratory experiments on samples of secondary calcite from Yucca Mountain, indicating that surface tension is effective for transport of water upwards to the tips of mineral crystals. On the basis of these observations, it is inferred that water flow into and through the lithophysae occurs as thin film flow along fractures intersecting the lithophysae and down the walls of the cavities. This inference is consistent with the results of Tokunaga and Wan (1997), who showed that film flow on fracture surfaces is an important flow mechanism in unsaturated tuff, especially at high relative humidities (e.g., low capillary suction).

As discussed in SAR Section 2.3.3.2.3.7.4, the occurrence of calcite and opal coatings on fractures and within lithophysal cavities corroborates the concept of a capillary barrier in two ways. First, many cavities do not contain secondary minerals and, hence, show no evidence of seepage or film flow leading to mineral deposition. Second, for cavities that contain calcite and opal, water flux into cavities, estimated from the amount of deposited minerals, is small relative to the estimated average percolation flux (Marshall et al. 2003, Section 5). Also, no correlation is found between the volume of secondary minerals and the size of the cavity (Marshall et al. 2003). Such a correlation would be expected for seepage into smooth-walled, cylindrical or spherical openings in homogeneous media (Philip et al. 1989; Knight et al. 1989). The fact that there is no correlation between secondary mineral quantity and cavity size is likely due to water entering the cavities as thin films via fractures. In most cases, lithophysae are intersected by fractures that may have served as fluid pathways. These can either be high-angle fractures cutting the cavity ceiling, or bedding-plane partings that extend short distances away from the lithophysae (Paces et al. 2001).

Although the distribution and abundance of calcite and opal in lithophysal cavities provides general corroboration for the drift seepage model (i.e., only a small fraction of lithophysae show any evidence of fluid entry, and the water volume entering is small relative to the total percolation flux), no quantitative comparison is possible, because water is assumed to enter lithophysal cavities by film flow. Seepage, as defined in seepage modeling for the TSPA, considers only dripping water. Similarly, the modeling of Philip et al. (1989) does not consider the effect of thin water films, either with respect to the hydrologic properties of the rock and conditions of seepage, or as a fraction of the water flowing into the cavity.

As part of the validation of the unsaturated zone flow models, one-dimensional simulation of calcite precipitation in the unsaturated zone was conducted to determine the sensitivity of calcite abundance to percolation flux (SNL 2007a, Section 7.7). The model treats fractures (including lithophysal cavities) and rock matrix as two separate continua, allowing for interaction. The model does not distinguish between fracture calcite and lithophysal cavity calcite. This is appropriate because, as noted above, the secondary calcite in the cavities is similar in texture to that found in fractures and, in some cases, there are fractures intersecting cavities with a continuous deposit of secondary minerals from the fracture into the cavity. The conclusion based on this analysis was that the percolation flux magnitude, and the extent of fracture-matrix interaction, are both described appropriately in the unsaturated zone flow models.

1.3 CONCLUSION

Percolating water enters lithophysal cavities as water films, based on lack of evidence for dripping. Film flow and its effects on seepage dripping into repository emplacement drifts is accounted for in the seepage model used for TSPA. Film flow as the predominant source of calcite and silica deposits in lithophysal cavities is consistent with the conceptual model for seepage into repository drifts, and with the interpretation of the laminar structure of those deposits. Therefore, no discrepancy or inconsistency exists in the seepage model conceptualization of capillary diversion around openings such as drifts, nor the use of the laminar layers of mineralization in lithophysae for the validation of percolation rate.

2. COMMITMENTS TO NRC

None.

3. DESCRIPTION OF PROPOSED LA CHANGE

None.

4. REFERENCES

BSC (Bechtel SAIC Company) 2004a. *Seepage Model for PA Including Drift Collapse.* MDL-NBS-HS-000002 REV 03. Las Vegas, Nevada: Bechtel SAIC Company. ACC: DOC.20040922.0008; DOC.20051205.0001.

BSC 2004b. *Seepage Calibration Model and Seepage Testing Data.* MDL-NBS-HS-000004 REV 03. Las Vegas, Nevada: Bechtel SAIC Company. ACC: DOC.20040922.0003; DOC.20060808.0003.

BSC 2005. *Drift-Scale Coupled Processes (DST and TH Seepage) Models.* MDL-NBS-HS-000015 REV 02. Las Vegas, Nevada: Bechtel SAIC Company. ACC: DOC.20050114.0004; DOC.20051115.0002.

Knight, J.H.; Philip, J.R.; and Waechter, R.T. 1989. "The Seepage Exclusion Problem for Spherical Cavities." *Water Resources Research*, *25*, (1), 29-37. Washington, D.C.: American Geophysical Union.

Marshall, B.D.; Neymark, L.A.; and Peterman, Z.E. 2003. "Estimation of Past Seepage Volumes from Calcite Distribution in the Topopah Spring Tuff, Yucca Mountain, Nevada." *Journal of Contaminant Hydrology*, *62-63*, 237-247. Amsterdam, The Netherlands: Elsevier.

Paces, J.B.; Neymark, L.A.; Marshall, B.D.; Whelan, J.F.; and Peterman, Z.E. 2001. *Ages and Origins of Calcite and Opal in the Exploratory Studies Facility Tunnel, Yucca Mountain, Nevada.* Water-Resources Investigations Report 01-4049. Denver, Colorado: U.S. Geological Survey. ACC: MOL.20020115.0207.

Philip, J.R.; Knight, J.H.; and Waechter, R.T. 1989. "Unsaturated Seepage and Subterranean Holes: Conspectus, and Exclusion Problem for Circular Cylindrical Cavities." *Water Resources Research, 25,* (1), 16-28. Washington, D.C.: American Geophysical Union.

SNL (Sandia National Laboratories) 2007a. *UZ Flow Models and Submodels.* MDL-NBS-HS-000006 REV 03 AD 01. Las Vegas, Nevada: Sandia National Laboratories. ACC: DOC.20080108.0003; DOC.20080114.0001; LLR.20080414.0007; LLR.20080414.0033; LLR.20080522.0086; DOC.20090330.0026[a].

SNL 2007b. *Abstraction of Drift Seepage.* MDL-NBS-HS-000019 REV 01 AD 01. Las Vegas, Nevada: Sandia National Laboratories. ACC: DOC.20070807.0001; DOC.20080813.0004; DOC.20081118.0049[b].

SNL 2008a. *Total System Performance Assessment Model /Analysis for the License Application.* MDL-WIS-PA-000005 REV 00 AD 01. Las Vegas, Nevada: Sandia National Laboratories. ACC: DOC.20080312.0001; LLR.20080414.0037; LLR.20080507.0002; LLR.20080522.0113; DOC.20080724.0005.

SNL 2008b. *Features, Events, and Processes for the Total System Performance Assessment: Analyses*. ANL-WIS-MD-000027 REV 00. Las Vegas, Nevada: Sandia National Laboratories. ACC: DOC.20080307.0003; DOC.20080407.0009; LLR.20080522.0166; DOC.20080722.0002.

Tokunaga, T.K. and Wan, J. 1997. "Water Film Flow Along Fracture Surfaces of Porous Rock." *Water Resources Research, 33,* (6), 1287-1295. Washington, D.C.: American Geophysical Union.

Whelan, J.F.; Paces, J.B.; and Peterman, Z.E. 2002. "Physical and Stable-Isotope Evidence for Formation of Secondary Calcite and Silica in the Unsaturated Zone, Yucca Mountain, Nevada." *Applied Geochemistry, 17,* (6), 735-750. New York, New York: Elsevier.

Whelan, J.F.; Paces, J.B.; Peterman, Z.E.; Marshall, B.D.; and Neymark, L.A. 2005. Erratum to "Reply to the comment on "Physical and stable-isotope evidence for formation of secondary calcite and silica in the unsaturated zone, Yucca Mountain, Nevada," by Y.V. Dublyansky, S.E. Smirnov, and G.P. Palyanova" [Applied Geochemistry 19 (2004) 1879-1889]. *Applied Geochemistry*, *20*, 1039-1050. New York, New York: Elsevier.

Whelan, J.F.; Paces, J.B.; Neymark, L.A.; Schmitt, A.K.; and Grove, M. 2006. "Impact of Quaternary Climate on Seepage at Yucca Mountain, Nevada." *Proceedings of the 11th International High-Level Radioactive Waste Management Conference, April 30 - May 4, 2006, Las Vegas, Nevada*. Pages 199-206. La Grange Park, Illinois: American Nuclear Society.

NOTES: [a]Provided as an enclosure to letter from Williams to Sulima, dtd 06/1/09, "Yucca Mountain – Request for Additional Information – Safety Evaluation Report, Volume 3 – Postclosure Chapter 2.2.1.3.6 – Flow Paths in the Unsaturated Zone, Set 1 – (Department of Energy's Safety Analysis Report Sections 2.3.2 and 2.3.3)."

[b]Provided as an enclosure to letter from Williams to Sulima dtd 02/17/2009. "Yucca Mountain – Request for Additional Information Re: License Application (Safety Analysis Report Section 2.1), Safety Evaluation Report Volume 3 – Postclosure Chapters 2.2.1.1 and 2.2.1.3.7 – Submittal of Department of Energy Reference Citations."

RAI Volume 3, Chapter 2.2.1.3.6, Second Set, Number 8:

Clarify how, or if, the fraction of the repository with liquid flux (seepage fraction) contacting the engineered components changes during a TSPA simulation. Also, if the change in the area of seeping environment is applied to the entire TSPA realization, describe the quantitative change in area for seepage environment when considering in-drift condensation. This information is needed to evaluate compliance with 10 CFR 63.114(a)(1,2,3).

Basis: Waste packages experiencing seepage at any time during a TSPA simulation are marked as being in the seeping environment for the entire simulation (SNL, 2008, Section 6.3.3.1.3). Seeping environment is defined to include areas with dripping (seepage) and areas with in-drift condensation (SAR Section 2.4.2.3.2.1.6). However, it is not clear if this tagging of marking waste packages also pertains to in-drift condensation, seismic ground motion and fault displacement, and igneous intrusion scenarios; i.e., do repository areas affected by in-drift condensation, seismic ground motion, and igneous activity cause a shift from non-seeping environment to a seeping environment for the entire TSPA realization? Also, 20,000- and million-year performance assessment simulations are discussed in the SAR (Section 2.4.2.2.2.2). It is not clear how the rule is applied for 10,000-yr results using the 20,000-yr simulations.

Also, the average quantitative change for the seepage environment (area denoted by seepage fraction plus condensation) is not clearly described when considering the process of in-drift condensation, as compared to seeping environment when not considering this process. Seepage fractions are reported in the SAR (e.g., Table 2.1-4), but areas affected by condensation are not presented.

1. RESPONSE

1.1 GENERAL DESCRIPTION OF LIQUID FLUX MODELING

Water contacting drip shields and waste packages is expected to originate from two sources: (1) drift seepage – seepage of groundwater from the unsaturated zone above the repository emplacement drifts; and (2) drift wall condensation – water-vapor condensate dripping from the walls of non-collapsed drifts (SAR Section 2.4.2.3.2.1.3). The TSPA model calculates drift seepage and drift wall condensation flow rates using the drift seepage submodel and the drift wall condensation submodel, respectively. These two flow rates are combined in the Engineered Barrier System (EBS) flow submodel (SAR Section 2.4.2.3.2.1.6) to yield a total dripping rate. As described in SAR Section 2.4.2.3.2.1.6, for each percolation subregion, the TSPA model includes two dripping environments: (1) the seeping environment, which applies a time dependent dripping rate above the waste packages that includes drift seepage; and (2) the non-seeping environment, which includes the waste packages that are not exposed to drift seepage (i.e., zero seepage flux). For each dripping environment (seeping and non-seeping), the TSPA model computes a time-dependent dripping rate equal to the sum of seepage and drift wall condensation. Only the seepage fraction, calculated in the drift seepage submodel as the ratio of

(1) waste packages impacted by a seepage rate greater than 0.1 kg/yr to (2) all waste packages in a percolation subregion by waste package type for a given realization, is used to define the number of waste packages in a seeping or non-seeping environment (SAR Section 2.3.3.4.2). Note that “dripping” and “seeping” are not synonymous.

Implementation of the Drift Seepage Submodel

In the TSPA model, implementation of repository-wide seepage conditions (e.g., seepage fraction and seepage rate) differs for the performance period analyzed (10,000 years or 1,000,000 years) and modeling case. For the 10,000-year performance period, the nominal, drip shield early failure, waste package early failure, and seismic ground motion modeling cases evaluate seepage conditions for the three climate states applicable to this time period (present-day, monsoon, and glacial-transition climates) using the non-collapsed drift seepage abstraction; the seismic fault displacement modeling case evaluates seepage conditions for the three climate states using the collapsed drift seepage abstraction. The igneous intrusion modeling case does not use the seepage abstraction after an igneous event; rather, this modeling case applies an average percolation flux for each climate state as the dripping rate at all waste package locations after the event has occurred (SAR Section 2.3.3.2.4). For the 10,000-year performance period, all TSPA modeling cases are calculated to 20,000 years in order to evaluate releases from commercial spent nuclear fuel (SNF) waste packages, whose in-package relative humidity rises above 95% (the threshold for release) between 9,000 and 14,000 years postclosure (SAR Section 2.4.2.3.2.2.2). This requires extending the glacial-transition climate to 20,000 years.

For the 1,000,000-year performance period, the nominal, drip shield early failure, and waste package early failure modeling cases evaluate seepage conditions for the three climate states (present-day, monsoon, glacial-transition) and also for the post-10,000-year representation of climate change as applicable to this time period, using the non-collapsed drift seepage abstraction; the seismic fault displacement modeling case evaluates seepage conditions for these climate states using the collapsed drift seepage abstraction; the seismic ground motion modeling case uses both the non-collapsed and collapsed drift seepage abstractions; and the igneous intrusion modeling case applies the percolation flux as the dripping rate at the repository horizon at all waste package locations after the event has occurred.

For all modeling cases and performance periods, the TSPA model determines a constant seepage fraction for each percolation subregion and each realization, based upon epistemically sampled parameters, and uses this seepage fraction to set the number of waste packages that are modeled within seeping and non-seeping environments (SAR Section 2.3.3.2.4). The seepage fraction is a constant value determined by the number of waste packages with any seepage during the three climate states (present-day, monsoon, and glacial-transition) for 10,000-year performance period or at any time during the 1,000,000-year performance period (see Table 5 in the response to RAI 3.2.2.1.3.6-2-010). The seepage fraction can be different for the two performance period calculations, even with the same sampling of epistemic parameter values, due to the generally wetter climate represented by the deep percolation rate used for the post-10,000-year calculation, as described in SAR Section 2.1.2.1 (i.e., the 1,000,000-year performance period cases will have higher seepage fractions). The seepage fraction varies among modeling cases and thus the number of waste packages in the seeping and non-seeping environment also varies between modeling cases.

Implementation of the Drift Wall Condensation Model

For each waste package type and percolation subregion, the drift wall condensation submodel estimates a time-dependent probability that condensation occurs, and a time-dependent condensation rate where condensation occurs. It is assumed that drift wall condensation can occur regardless of the presence or absence of seepage, and that condensation occurs independently among waste packages. The condensate dripping from drift walls is accounted for in TSPA calculations by adding the average condensation rate (fraction of waste packages having condensation multiplied by the condensation rate) to the drift seepage volumetric flow rate (which may be zero in the non-seeping environments) to calculate a dripping rate. Drift wall condensation does not change the fraction of waste packages in a seeping or non-seeping environment.

The drift wall condensation rate and the drift wall condensation fraction results for the first 2,000 years of the postclosure period are presented in SAR Tables 2.1-10 and 2.1-11. Drift wall condensation ceases after 2,000 years for commercial spent nuclear fuel and codisposal waste packages and does not recur.

1.2 MODELING CASE SPECIFIC CONSIDERATIONS FOR SEEPAGE CALCULATIONS

Nominal and Early Failure Modeling Cases and the 10,000-Year Seismic Ground Motion Modeling Case

The drift seepage abstraction for non-collapsed drifts is applied in the 10,000-year performance period for the nominal modeling case, the drip shield and the waste package early failure modeling cases, and the seismic ground motion modeling case. This abstraction is also applied in the 1,000,000-year performance period for the nominal modeling case, and the drip shield and the waste package early failure modeling cases. Each of these modeling cases excludes the explicit effects of drift collapse on the performance of the repository; however, the drift seepage abstraction for non-collapsed drifts includes a seepage rate multiplier of 1.2 (i.e., an increase of 20%). This increase accounts for non-collaped drifts that have moderately degraded (for example after local wedge-type rockfall in nonlithophysal rock) and the associated uncertainty in the seepage prediction (SAR Section 2.3.3.2.3.6.4).

Seismic Fault Displacement Modeling Cases

The drift seepage abstraction for collapsed drifts is applied to both the 10,000-year and 1,000,000-year calculations of the seismic fault displacement modeling case. The seepage rate and seepage fraction for the 10,000-year cases only involves the climate changes up to 10,000 years. There are waste package locations that are only impacted by seepage after 10,000 years. For the 10,000-year calculations, these waste packages are excluded from the seeping environment, and to maintain consistency, the climate change at 10,000 years is not applied. In addition, the expected dose prior to and at 10,000 years is determined using numerical integration (quadrature) that involves interpolation between the consequences of events that occur before and after 10,000 years. If the seepage calculations for later events included the climate change at 10,000 years, then the expected dose at 10,000 years would be influenced by the climate change that occurs after 10,000 years. The climate change at 10,000 years is excluded from the 10,000-year performance evaluations to mitigate both of these influences (SNL 2008, Sections 6.6.2.1 and 6.6.2.2). The 1,000,000-year modeling case includes the effects of all modeled climate states.

Igneous Intrusion Modeling Cases

In the igneous intrusion modeling case, the drift seepage abstraction for non-collapsed drifts is used to group waste packages into the seeping and non-seeping environments. Prior to the igneous event, this abstraction is also used to determine the average seepage rate for each waste package group. Although the drift seepage abstraction for non-collapsed drifts is used to determine the seepage fraction for placing waste packages into the seeping or non-seeping environments, this placement is only applicable to conditions prior to the igneous event. After the igneous intrusion event has occurred, every waste package location in the repository, whether in a seeping environment or a non-seeping environment, is exposed to a liquid flux and the applicable abstractions for seeping conditions in the EBS are applied in both the seeping and non-seeping environments; therefore, the effective seepage fraction becomes 100% (SNL 2008, Section 6.3.3.1.2). This is modeled by applying dripping specific submodels (e.g., the liquid influx in-package chemistry abstraction) instead of non-dripping specific submodels (e.g., the vapor influx in-package chemistry abstraction), not by moving waste packages between seeping and non-seeping groups. A post-event dripping rate is calculated for each percolation subregion that is equal to the average percolation flux in the percolation subregion; which is applied to waste packages in both the seeping and non-seeping environments.

1,000,000-Year Seismic Ground Motion Modeling Case

The drift seepage abstractions for non-collapsed and collapsed drifts are both used to determine seepage conditions for the 1,000,000-year seismic ground motion modeling case. As in the other cases, separate seepage rates and seepage fractions are calculated for the waste package groups of each fuel type and percolation subregion combination. Whether the non-collapsed drift abstraction results or the collapsed drift abstraction results are applied depends on the integrity of the drift after each seismic event. In the 1,000,000-year seismic ground motion modeling case, the sequence of seismic events that will occur during each simulation is determined before the seepage calculations are performed. When evaluating the sequence of events, the damage to the drift after each event is calculated and the cumulative volume of lithophysal and nonlithophysal rubble that will collapse as a result of the events is determined before the seepage calculations are performed. If the cumulative volume of lithophysal rubble that collapses by the end of the 1,000,000-year period exceeds 5 m^3/m over the simulated duration, the seepage fraction contribution from waste packages in the lithophysal region is determined from the collapsed drift abstraction results. If the cumulative volume of lithophysal rubble does not exceed the 5 m^3/m threshold, the seepage fraction contribution from the waste packages in the lithophysal region is determined from the non-collapsed drift abstraction results. If the cumulative volume of nonlithophysal rubble that collapses exceeds 0.5 m^3/m over the simulated duration, the seepage fraction contribution from the waste packages in the nonlithophysal region is determined from the collapsed drift abstraction. If the maximum volume of nonlithophysal rubble does not exceed the 0.5 m^3/m threshold, the seepage fraction contribution of the nonlithophysal waste packages is determined from the non-collapsed drift abstraction (SNL 2008, Section 6.3.3.1.3). For both rock types, the seepage rate is interpolated from the non-collapsed drift and collapsed drift results using the time-dependent cumulative volume of rubble that collapses into the drift as the interpolation parameter. Although seepage rates for waste packages in lithophysal and non-lithophysal regions may be calculated from different abstractions, the net seepage fraction is still the ratio of (1) the number of waste packages impacted by seepage above the 0.1 kg/yr threshold to (2) the total number of waste packages in the waste package group. Note that drift degradation results in a significant increase in the fraction of waste packages that encounter seeping conditions, from 40% to 69% based on the increase in the seepage fraction (SAR Section 2.4.2.2.1.2.2.1).

1.3 MODELING CASE SPECIFIC CONSIDERATIONS FOR IN-DRIFT CONDENSATION

Condensation in open drifts is predicted to occur up to about 2,000 years after closure. Drift wall condensation is calculated using regressions of condensation rate and condensation probability in an emplacement drift to average percolation rate in the drift (SNL 2008, Section 6.3.3.2.2). The regression response surface for probability of condensation in a drift is equated to the fraction of waste package locations that have condensation in a percolation subregion by using the average percolation rate in a subregion as input to the condensation response surface. The drift wall condensation submodel predicts no significant condensation after 2,000 years (SNL 2008, Section 6.3.3.2.2).

For the Seismic Scenario Class, there is no condensation in the lithophysal units after drift collapse. Thus, for the 10,000-year seismic fault displacement and 1,000,000-year seismic fault displacement modeling cases, dripping rates do not include condensation at waste package locations in the lithophysal units (SNL 2008, Section 6.3.3.2.2). For the 1,000,000-year seismic ground motion modeling case, dripping rates may or may not include condensation at waste package locations in the lithophysal units, depending on the cumulative rockfall caused by seismic events. For the 10,000-year seismic ground motion modeling case, drift collapse does not occur and the condensation submodel is evaluated the same as in the nominal and early failure modeling cases.

The condensation model is not applied to the igneous intrusion modeling case after an igneous intrusion event, since condensation is not expected to occur in magma-filled drifts. Prior to an igneous intrusion event, the condensation model is evaluated as in the nominal and early failure modeling cases (SAR Section 2.4.2.3.2.1.12.2).

1.4 SUMMARY

The seeping environment includes all of the waste packages subjected to drift seepage, whereas the non-seeping environment includes those without seepage. In-drift condensation is added to the dripping rate over waste packages in both the seeping and non-seeping environments. For all modeling cases, the seepage fraction is determined once per realization and is not time dependent. The dripping rate (e.g., seepage plus in-drift condensation) changes with time as a result of changes in climate, the presence of condensation, and drift collapse. There is no change to the fraction of waste packages in a seeping environment (e.g., seepage fraction) when considering in-drift condensation. In the igneous intrusion modeling case, the seepage fraction does not change; rather, after the event the dripping rate (equal to the percolation flux) is applied to both the seeping and non-seeping environments. Tables 1 and 2 summarize the seepage fraction and in-drift condensation utilized for the TSPA modeling cases and performance periods.

Table 1. Fraction of Waste Packages in a Seeping Environment for TSPA Modeling Cases and Performance Periods

Modeling Case	Fraction of Waste Packages in a Seeping Environment	
	10,000-Year Performance Period	1,000,000-Year Performance Period
Nominal	Nominal seepage fraction at 10,000 years	Nominal seepage fraction at 1,000,000 years
Drip Shield Early Failure	Nominal seepage fraction at 10,000 years	Nominal seepage fraction at 1,000,000 years
Waste Package Early Failure	Nominal seepage fraction at 10,000 years	Nominal seepage fraction at 1,000,000 years
Seismic Fault Displacement	Collapsed drift seepage fraction at 10,000 years	Collapsed drift seepage fraction at 1,000,000 years
Seismic Ground Motion	Nominal seepage fraction at 10,000 years	Seepage fraction at 1,000,000 years accounting for cumulative effects of drift collapse
Volcanic Eruption	No Groundwater Transport	
Igneous Intrusion	Nominal seepage fraction at 10,000 years up to the time of the event. After the event, a dripping rate equal to the percolation flux is applied to 100% of the waste package locations.	Nominal seepage fraction at 1,000,000 years up to the time of the event. After the event, a dripping rate equal to the percolation flux is applied to 100% of the waste package locations.

Table 2. Drift Wall Condensation for TSPA Modeling Cases and Performance Periods

Modeling Case	Duration of the TSPA Simulation	
	10,000-Year Performance Period	1,000,000-Year Performance Period
Nominal	Drift wall condensation may occur during first 2,000 years postclosure.	
Drip Shield Early Failure	Drift wall condensation may occur during first 2,000 years postclosure.	
Waste Package Early Failure	Drift wall condensation may occur during first 2,000 years postclosure.	
Seismic Fault Displacement	Drift wall condensation may occur during first 2,000 years postclosure. Does not occur for waste packages in the lithophysal units due to drift collapse.	
Seismic Ground Motion	Drift wall condensation may occur during first 2,000 years postclosure.	Drift wall condensation may occur during first 2,000 years postclosure as long as lithophysal drift collapse does not occur.
Volcanic Eruption	No Groundwater Transport	
Igneous Intrusion	Drift wall condensation may occur during first 2,000 years postclosure prior to an igneous event. Does not occur after igneous intrusion event.	

2. COMMITMENTS TO NRC

None.

3. DESCRIPTION OF PROPOSED LA CHANGE

None.

4. REFERENCES

SNL (Sandia National Laboratories) 2008. *Total System Performance Assessment Model/Analysis for the License Application*. MDL-WIS-PA-000005 REV 00 AD 01. Las Vegas, Nevada: Sandia National Laboratories. ACC: DOC.20080312.0001; LLR.20080414.0037; LLR.20080507.0002; LLR.20080522.0113; DOC.20080724.0005.

RAI Volume 3, Chapter 2.2.1.3.6, Second Set, Number 10:

Explain how average seepage rates and fractions vary or do not vary for different TSPA scenarios for the pre-10,000-yr glacial transition and post-10,000-yr climates. Also explain how uncertainties in seepage rates and fractions vary by scenario for the entire repository for the pre-10,000-yr glacial transition and post-10,000-yr climates.

To support the explanations, provide a table of seepage rates in the seeping environments, seepage percentages, and seepage fractions for the glacial transition and post-10,000 year climates. The table should include nominal/early failure, seismic ground motion, seismic fault displacement, and igneous intrusion TSPA-LA modeling cases. The table should list values of repository-wide average and range (e.g., fifth and ninety-fifth percentiles).

This information is needed to determine compliance with 10 CFR 63.114(a)(1,2,7).

Basis: DOE presents a log-log plot (SAR Figure 2.1-5) to illustrate the time dependent seepage rates for nominal and seismic ground motion modeling cases as calculated by TSPA-LA. Four tables in the SAR, 2.1-6 to 2.1-9, provide the seepage fractions for drifts containing the DOE co-disposed high-level wastes and commercial spent nuclear fuel wastes with respect to the aforementioned modeling cases at 10,000 and 1,000,000 years. Example seepage calculations are also provided in SAR 2.3.3.4.2 for intact and collapsed drifts. In the same SAR section, DOE states that '*[r]esults from this calculation are not utilized in the TSPA*.' The cited seepage rates, percentages, and fractions in the example calculations are helpful in demonstrating barrier capabilities and TSPA-LA seepage calculations. However, they are not the final results from TSPA-LA modeling cases that are required to demonstrate compliance.

This request for additional information is related to that for Request for Additional Information (RAI) for Volume 3 (Postclosure), Chapter 2.2.1.3.6 (Unsaturated Zone Flow), Set 1, RAI #5. Whereas averages of the five percolation bins may be provided for Set 1, RAI #5, repository-wide averages and ranges calculated from the thousands of seepage locations are requested in this new RAI.

1. RESPONSE

In the total system performance assessment (TSPA) model, seepage conditions (e.g., seepage fraction, seepage rate, and seepage percentage) are defined for the duration of the performance period (10,000 years or 1,000,000 years) and are impacted by the consequences of disruptive events (SAR Section 2.3.3.2.4.2).

10,000-year time period—For the 10,000-year analyses, the nominal, drip shield early failure, waste package early failure, and seismic ground motion modeling cases evaluate seepage conditions for three climate states (present-day, monsoon, and glacial-transition) using the non-collapsed drift seepage abstraction; and the seismic fault displacement modeling case evaluates seepage conditions for the three climate states using the collapsed drift seepage abstraction. The igneous intrusion modeling case does not use the seepage abstraction after an igneous event; rather, this modeling case applies an average percolation flux for each climate state as the dripping rate at all waste package locations after the event has occurred (SAR Section 2.3.3.2.4). For the 10,000-year performance period, all TSPA modeling cases are calculated to 20,000 years in order to demonstrate stability and to examine the failure of commercial spent nuclear fuel (SNF) waste packages, whose in-package relative humidity does not rise above 95% (the threshold for release) until around 10,000-years (SAR Section 2.4.2.3.2.2.2). This requires extending the glacial-transition climate to 20,000 years.

1,000,000-year time period—For the 1,000,000-year analyses, the nominal, drip shield early failure, and waste package early failure modeling cases evaluate seepage conditions for the three climate states (present-day, monsoon, glacial-transition) and the post-10,000-year representation of climate change using the non-collapsed drift seepage abstraction. The seismic fault displacement modeling case evaluates seepage conditions for these four climates using the collapsed drift seepage abstraction. The seismic ground motion modeling case applies both the non-collapsed and collapsed drift seepage abstractions, as described in Section 1.5. The igneous intrusion modeling case applies the percolation flux as the dripping rate at the repository horizon at all waste package locations after the igneous intrusion event has occurred.

Although different TSPA modeling cases implement different seepage calculation methods, the epistemic parameters common between calculation methods (e.g., infiltration, seepage uncertainty, capillary strength uncertainty, and permeability uncertainty) apply the same sampled values for all modeling cases and for both model durations. Furthermore, within an epistemic realization, spatial variability parameters common between calculation methods (e.g., percolation flux variability, flow focusing factor variability, permeability variability, and capillary strength variability) also apply the same sampled values.

For all modeling cases and performance periods, the TSPA model determines a constant seepage fraction for each percolation subregion and each realization, based upon epistemically sampled parameters, and uses this seepage fraction to set the number of waste packages that are modeled within seeping and non-seeping environments (SAR Section 2.3.3.2.4). The seepage fraction is a constant value determined by the number of waste packages with any seepage during the three climate states (present-day, monsoon, and glacial-transition) for 10,000-year performance period or at any time during the 1,000,000-year performance period. The seepage fraction can be different for the two performance period calculations, even with the same sampling of epistemic parameter values, due to the generally wetter climate represented by the deep percolation rate used for the post-10,000-year calculation (i.e., the 1,000,000-year performance period cases will have higher seepage fractions). The seepage fraction varies among modeling cases and thus the number of waste packages in the seeping and non-seeping environment also varies between modeling cases.

Quantitative values for the repository-wide seepage fraction, seepage rate, and seepage percentage are reported for the different TSPA modeling cases. For each epistemic realization of the TSPA model, seepage rates and seepage fractions are determined and reported for five different percolation subregions for commercial SNF and codisposal waste packages. Each of the ten reported seepage rates is the average seepage rate of hundreds to thousands of spatially variable seepage calculations. Repository-wide seepage fractions, seepage rates, and seepage percentages are determined from these results. These results expand upon previously reported values for these parameters (SAR Tables 2.1-6 through 2.1-9; SAR Figure 2.1-5; and Table 11 of the response to RAI 3.2.2.1.3.6-005) by providing repository-wide averages, by including additional modeling cases, and by presenting a range of epistemic uncertainty for these quantities.

1.1 SEEPAGE FRACTION, SEEPAGE RATE, AND SEEPAGE PERCENTAGE

Seepage conditions vary by TSPA modeling case and model duration and these variations are characterized by the seepage fraction, the seepage rate, and the seepage percentage (the ratio of the seepage flux to the percolation flux). In the TSPA model, the repository performance is modeled using groups of waste packages with common characteristics (SNL 2008, Section 6.1.5.3). Two common characteristics are waste package type and percolation subregion. The two waste package types (commercial SNF waste packages and codisposal waste packages) are modeled in five different percolation subregions. A third grouping characteristic places waste packages within each waste package type/percolation subregion group into seeping and non-seeping environments. Waste packages at drift locations that seep at any time during the performance period are modeled in the seeping environment. All other waste packages are modeled in the non-seeping environment. As summarized in Tables 1 and 2 of the response to RAI 3.2.2.1.3.6-2-008, the seepage fraction used to calculate the number of waste packages in the seeping environment excludes the contribution of drift wall condensation so that the seepage fraction and dripping fraction are not the same values.

The number of waste packages in each percolation subregion environment is determined by the seepage fraction, which may be different for different modeling durations and cases. Therefore, a waste package location that is modeled in the non-seeping environment in one modeling case may be modeled in the seeping environment in a separate modeling case that applies a different seepage model. For the same modeling case, a waste package location that is modeled in the non-seeping environment for the 10,000-year analysis may be modeled in the seeping environment for the 1,000,000-year analysis. The seepage fraction for the 1,000,000-year analysis will be greater than or equal to the seepage fraction in the 10,000-year analysis. If seepage occurs at a waste package location in the first 10,000 years of the 10,000-year analysis, it will also occur in the first 10,000 years of the 1,000,000-year analysis and therefore will be a seeping location for both durations.

In the TSPA model, waste package group assignments are determined prior to assessing the capability of the Engineered Barrier System (EBS) to retain the waste. The fraction of the waste packages that belong to each waste package type and percolation subregion are specified and do not change. The fraction of waste packages modeled in the seeping and non-seeping environments is determined at the beginning of each realization by calling a dynamically linked library (DLL), the seepage DLL, to perform seepage calculations spanning the performance period. The TSPA model calls the seepage DLL with sampled values for uncertain parameters and ranges for spatial variability parameters, and the DLL evaluates the seepage abstractions and returns a time history of seepage through the repository and the fraction of waste packages that are exposed to seepage during the performance period. Within the seepage DLL, a separate calculation is performed for each waste package type and percolation subregion for the non-collapsed drift, collapsed drift, and igneous intrusion conditions. Conditional on the modeling case and the state of the drift at the end of the simulation, the TSPA model uses the non-collapsed drift or collapsed drift seepage fraction for each waste package type and percolation subregion group to determine the number of waste packages that are assigned to the seeping environment. The number of waste packages assigned to the seeping environment is equal to the product of the seepage fraction for the group and the total number of waste packages in the group. The balance of the waste packages in the group is assigned to the non-seeping environment. Because the seepage fraction includes all waste packages where seepage occurs at any time during the performance period, the seepage fraction is constant within a TSPA model realization and the number of waste packages assigned to the seeping and non-seeping environments does not vary while the performance of the repository is evaluated.

In addition to calculating seepage fractions for each waste package type and percolation subregion group, the seepage DLL also calculates the average seepage rate for each seeping environment. Multiple calls to the seepage DLL produce time histories of average seepage rates per waste package location for non-collapsed drift and collapsed drift conditions. The seepage rates returned by the seepage DLL are the average rates from all of the waste package locations that yield a seepage rate above the seepage threshold of 0.1 kg/yr. For each epistemic realization, the average seepage rates calculated by the seepage DLL account for uncertainty in a number of parameters including: the capillary strength, the infiltration scenario used to specify the range of percolations fluxes, the permeability, and the seepage rate. In addition to uncertainty, the average seepage rates calculated by the seepage DLL also account for spatial variability in the values of capillary strength, permeability, flow focusing factor, and percolation flux. For each percolation subregion and waste package type, the seepage DLL evaluates from 326 to 7,800 spatially variable combinations of parameters for each epistemic sample and climate and returns the average seepage rate from all of the waste package locations that yield a seepage rate above the seepage threshold of 0.1 kg/yr. Table 1 identifies the number of spatial variability samples applied for each epistemic sample for each percolation subregion and waste package type. The number of spatial variability samples is determined by the number of histories captured in the comprehensive thermal hydrology set, which is the source of the percolation rates and temperatures used by the seepage DLL. Table 2 provides the range of uncertain parameters and variability parameters applied in the seepage calculations performed within the TSPA model. Table 3 provides the range of percolation flux values used in the seepage calculations. For each TSPA modeling case, the seepage DLL calculates seepage rates at approximately 15.7 million spatially variable locations (2 drift collapse states × 26,112 samples per epistemic realization × 300 epistemic realizations) for each of the four climates (present-day, monsoon, glacial-transition, and the post-10,000-year representation of climate change) in a 1,000,000-year analysis and for each of the three climates states (present-day, monsoon, glacial-transition) for the 10,000-year analysis. In addition to these calculations, the seepage DLL also records the percolation rate applied in each calculation and can report the average percolation rates for each percolation subregion and waste package type when instructed to report these values.

Table 1. Number of Spatial Variability Samples Evaluated by the Seepage DLL for Each Epistemic Sample and Climate

Waste Package Type	Percolation Subregion Number	Number of Samples
Commercial SNF	1	978
Commercial SNF	2	4,902
Commercial SNF	3	7,800
Commercial SNF	4	4,920
Commercial SNF	5	984
Codisposal	1	326
Codisposal	2	1,634
Codisposal	3	2,600
Codisposal	4	1,640
Codisposal	5	328

Table 2. Distribution of Epistemic Uncertainty and Spatial Variability Parameters Used in the Drift Seepage Submodel

Parameter	Epistemic Uncertainty	Spatial Variability	Applied Value
Infiltration (10th-percentile map, 30th-percentile map, 50th-percentile map, 90th-percentile map)	Discrete (0.6191, 0.1568, 0.1645, 0.0596) (from SAR Sections 2.4.2.3.2.1.1 and 2.4.2.3.2.1.2)	None	Not Applicable. Used to determine the set of percolation flux values.
Percolation flux (mm/yr)	Determined by sampled infiltration map	See Table 3	Extracted from thermal hydrology input file for the sampled infiltration scenario
Capillary strength (Pa)	Triangular[a] (Min: −105 Pa; Most Likely: 0 Pa; Max: 105 Pa)	Uniform[a] (402 Pa, 780 Pa)	Epistemic Sample + Variability Sample
Permeability (m^2) (log value) Lithopysal locations	Triangular[a] (Min: −0.92; Most Likely: 0; Max: 0.92)	Normal[a] (μ: -11.5; σ: 0.47)	Epistemic Sample + Variability Sample
Permeability (m^2) (log value) Nonlithopysal locations	Triangular[a] (Min: −0.68; Most Likely: 0; Max: 0.68)	Normal[a] (μ: -12.2; σ: 0.34)	Epistemic Sample + Variability Sample
Flow focus factor	None	CDF (Min: 0.116; Max: 5.016)[b] (represented as a polynomial)	Variability Sample
Seepage uncertainty	Uniform (−1.7321, 1.7321)	None	Mean(SV) + Epistemic Sample × Standard Deviation(SV)[c]

[a] Values are sampled independently for lithophysal and nonlithophysal locations.

[b] Source: SNL 2007, Section 6.6.5.2 (p. 6-154), Figure 6.6-15.

[c] The seepage uncertainty is multiplied by the spatially variable standard deviation for the mean seepage rate and the result is added to the spatially variable mean seepage rate. The mean and standard deviation values are determined from the Seepage Model for Performance Assessment lookup tables using the applied values for capillary strength, permeability, and the percolation flux adjusted for flow focusing.

When considering the non-collapsed drift and collapsed drift calculations performed by the seepage DLL, the values of the uncertain parameters are the same for the non-collapsed drift and collapsed drift calculations. For each spatially variable calculation within one epistemic realization, the values of the spatial variability parameters used in the non-collapsed drift and collapsed drift scenarios are also the same. However, for different epistemic realizations, all uncertain parameters and all spatial variability parameters are re-sampled. Between TSPA modeling cases, the same epistemic samples and spatial variability samples are applied. Therefore, the treatment of uncertainty and spatial variability in the seepage calculations is consistent across all but one of the modeling cases. The exception is the igneous intrusion modeling case, which does not apply the non-collapsed drift nor the collapsed drift seepage abstraction. The liquid flux rate applied to each waste package group in the igneous intrusion case is derived from the average percolation flux as shown in Table 3. Sampled values for the uncertainty in the infiltration scenario used to select the range of percolation fluxes applied in the igneous intrusion modeling case are the same as those applied in the seepage calculations performed in the other modeling cases. Therefore, the percolation rates used to determine the flux rate at the repository horizon in the igneous intrusion modeling case are the same as the percolation rates used to determine seepage in the other modeling cases.

As detailed in the response to RAI 3.2.2.1.3.6-004, the average seepage rate from the spatial variability results generally exceeds the median value of the spatially variable values. Therefore, the seepage rate applied to the waste package group, as a whole, generally overestimates the liquid flux rate onto an individual waste package. The uncertainty in the average seepage rate and seepage fraction is governed by both epistemic uncertainty and spatial variability. However, in the TSPA model, the applied seepage rate has been averaged over tens to thousands of spatially variable values. To this extent, the quantitative values presented in the remainder of this RAI response only address the uncertainty in the average seepage rate and the seepage fraction and do not address variability as variability is removed from the results due to the averaging that is applied.

Table 3. Range of Percolation Rates by Percolation Subregion and Infiltration Map

		Range of Percolation Rates (mm/yr) (Lower / Median / Upper / Mean)															
		Present-Day				**Monsoon**				**Glacial-Transition**				**Post-10,000-Year**			
Infiltration	**Subregion**	Min	Median	Max	**Avg**	Min	Median	Max	**Avg**	Min	Median	Max	**Avg**	Min	Median	Max	**Avg**
10th-percentile map	1	0.133	0.445	1.25	**0.489**	0.427	1.01	5.04	**1.23**	0.153	0.646	1.30	**0.682**	0.664	1.89	14.8	**2.56**
	2	0.607	2.47	4.43	**2.33**	1.12	5.56	9.53	**5.38**	1.32	3.74	6.27	**3.72**	2.05	16.5	26.6	**15.1**
	3	1.94	4.32	6.34	**4.32**	3.61	8.43	11.2	**8.31**	6.27	11.2	16.1	**11.1**	9.91	23.7	33.4	**23.3**
	4	4.15	5.70	6.96	**5.68**	7.32	9.91	12.7	**10.0**	16.2	20.8	26.9	**20.9**	20.7	26.9	36.6	**26.9**
	5	5.96	6.53	8.1	**6.71**	10.4	11.2	14.6	**11.7**	27.2	30.1	36.2	**30.5**	26.3	30.6	37.5	**30.9**
30th-percentile map	1	0.344	1.37	4.83	**1.58**	0.552	1.96	10.1	**2.34**	0.426	2.23	9.20	**2.51**	0.395	2.42	6.20	**2.55**
	2	1.65	7.00	14.7	**6.50**	2.33	10.9	25.6	**10.7**	3.57	14.2	32.0	**13.5**	4.44	18.3	40.6	**17.5**
	3	3.41	10.8	15.7	**10.8**	6.51	16.9	27.9	**17.0**	11.0	27.4	39.8	**27.1**	18.5	41.3	61.5	**41.5**
	4	8.12	13.7	17.3	**13.6**	13.3	20.8	31.2	**21.2**	25.9	38.5	49.1	**38.3**	38.7	62.8	77.4	**61.6**
	5	14.0	15.3	19.0	**15.8**	19.7	24.4	27.9	**24.1**	38.3	47.1	54.9	**46.9**	68.2	77.8	89.3	**77.8**
50th-percentile map	1	0.595	2.00	7.20	**2.22**	0.527	2.30	5.80	**2.29**	0.449	2.30	5.24	**2.45**	0.856	3.79	11.0	**4.30**
	2	2.15	10.2	19.9	**9.76**	2.50	11.4	25.7	**11.2**	3.67	16.5	36.0	**15.7**	5.68	31.2	62.2	**29.9**
	3	6.70	15.8	22.1	**15.6**	10.3	20.4	32.4	**20.4**	16.5	36.9	55.1	**37.2**	24.1	56.6	79.5	**55.7**
	4	13.7	18.9	26.6	**18.9**	20.5	26.1	37.7	**26.6**	37.8	56.3	69.4	**55.1**	53.2	71.0	95.6	**70.5**
	5	20.0	22.9	25.8	**22.8**	29.6	35.4	49.9	**36.1**	61.0	69.7	79.9	**69.6**	74.2	82.6	101	**84.3**
90th-percentile map	1	1.32	4.11	19.2	**4.94**	3.08	9.27	60.6	**12.5**	1.20	5.50	14.3	**5.84**	2.31	7.02	38.8	**8.81**
	2	3.45	26.3	45.5	**24.1**	10.3	71.2	118	**65.4**	7.69	42.3	80.9	**40.3**	7.48	47.4	80.8	**43.7**
	3	15.2	37.2	52.6	**36.9**	43.9	102	142	**99.9**	32.5	76.1	108	**74.9**	29.1	67.6	93.9	**66.6**
	4	32.0	42.3	57.9	**42.5**	87.8	115	159	**116**	71.9	95.4	129	**94.8**	58.8	76.4	106	**76.9**
	5	41.7	47.4	58.7	**48.6**	113	128	160	**132**	100	110	136	**113**	75.0	85.0	106	**87.5**

NOTE: The mean percolation rate for the 50th-percentile infiltration case, present-day climate in repository percolation subregion #2 was incorrectly reported to be 9.72 mm/yr in Table 4 of the response to RAI 3.2.2.1.3.6-005. Table 3 contains the correct value and Attachment 1 of this response provides the corrected Table 4 for the response to RAI 3.2.2.1.3.6-005.

.

In addition to the seepage fraction, another quantitative value that is useful for assessing the capability of the Upper Natural Barrier for diverting flow from the repository is the seepage percentage. The seepage percentage is the ratio between the seepage rate and the percolation flux arriving over the footprint of the considered drift segment (SAR Section 2.3.3.2.3.4.1). A seepage percentage of 100% means that there is no flow diversion capability of the drift and the natural system between the drift and the base of the Paintbrush Tuff nonwelded (PTn) unit. A seepage percentage of 0% means that all flow from the base of the PTn unit is diverted around the drifts. Although not directly reported by the seepage DLL, quantitative values for the seepage percentage, including the range of epistemic uncertainty, can be determined for the different seepage calculations. For non-collapsed conditions, the percolation flux used to calculate the seepage percentage is the average percolation flux over one drift segment, defined as the product of the intact drift diameter and the applied waste package length. For the collapsed drift calculations, this area is increased by a factor of two to account for the increased drift diameter after collapse.

1.2 SEEPAGE CALCULATIONS FOR NOMINAL MODELING CASES

The drift seepage abstraction for non-collapsed drifts (SAR Section 2.3.3.2.3.4.1) is applied in the 10,000-year calculations of the nominal modeling case, the drip shield and the waste package early failure modeling cases, and the seismic ground motion modeling case. In each of these modeling cases, nominal drift conditions prevail and the drift is not subjected to disruptive events that result in drift collapse. This abstraction is also applied in the 1,000,000-year calculations of the nominal modeling case, and the drip shield and the waste package early failure modeling cases. Each of these modeling cases excludes the explicit effects of drift collapse on the performance of the repository; however, the drift seepage abstraction for non-collapsed drifts includes a seepage rate multiplier of 1.2 (i.e., an increase of 20%). This increase accounts for non-collapsed drifts that have moderately degraded (e.g., after local wedge-type rockfall in nonlithophysal rock), and the associated uncertainty in the seepage prediction (SAR Section 2.3.3.2.3.6.4).

In the TSPA model, seepage fractions and seepage rates for non-collapsed drift conditions are calculated for five percolation subregion groups for both commercial SNF and codisposal waste packages. The repository-wide average seepage fraction and seepage rate combine these results into one seepage fraction and one seepage rate history. The repository-wide seepage fraction is the sum of the seepage fractions from the ten waste package groups weighted by the relative size of each group. The repository-wide average seepage rate is the total annual seepage that enters the repository divided by the total number of waste packages in the repository (see Equation 1). The repository-wide average seepage rate for waste packages in the seeping environments is the total annual seepage that enters the repository divided by the total number of waste packages in the seeping environments (see Equation 2).

$$\overline{Q}_{seep} = \frac{\sum_{i=1}^{2}\sum_{j=1}^{5} N_{wp} \times f_i \times f_j \times f_{seep,ij} \times Q_{seep,ij}}{N_{wp}} \qquad \text{(Eq. 1)}$$

$$\overline{Q}_{seep}^{seeponly} = \frac{\sum_{i=1}^{2}\sum_{j=1}^{5} N_{wp} \times f_i \times f_j \times f_{seep,ij} \times Q_{seep,ij}}{\sum_{i=1}^{2}\sum_{j=1}^{5} N_{wp} \times f_i \times f_j \times f_{seep,ij}} \qquad \text{(Eq. 2)}$$

where

$\overline{Q}_{seep}$	is the repository-wide average seepage rate (m^3/yr) per waste package location.
$\overline{Q}_{seep}^{seeponly}$	is the repository-wide average seepage rate (m^3/yr) per waste package location for those waste packages that are in the seeping environment.
N_{wp}	is the total number of waste packages (=11,629).
f_i	is the fraction of waste packages of each type i (1 = commercial SNF, 2 = codisposal).
f_j	is the fraction of the repository assigned to each percolation subregion.
$f_{seep,ij}$	is the seepage fraction of the waste packages of type i in percolation subregion j.
$Q_{seep,ij}$	is the spatially averaged seepage rate per waste package location for the seeping environment of the waste packages of type i in percolation subregion j.

For each epistemic sample, the repository-wide seepage rate per waste package location is calculated using Equation 1 and the repository-wide seepage rate per waste package location for seeping locations is calculated using Equation 2. From these results, the average and selected quantiles are tabulated in Table 4 for 10,000-year analyses and Table 5 for 1,000,000-year analyses. Table 4 also provides the uncertainty range for the repository-wide average seepage fraction and seepage percentage for the 10,000-year cases that apply the non-collapsed drift seepage calculations. Table 5 provides the analogous results for 1,000,000-year cases.

The seepage rate and seepage fraction for the 10,000-year analyses, which are run to 20,000 years, only include the climate changes up to 10,000 years. In these analyses, the glacial-transition climate is extended to 20,000 years. The seepage fraction increases with the inclusion of the post-10,000-year climate change. Therefore, there are waste package locations where seepage only occurs after 10,000 years. For the 10,000-year analyses, these waste packages are excluded from the seeping environment and, to maintain consistency, the climate change at 10,000 years is not applied. The decrease in the seepage rate for the glacial-transition climate between the 10,000-year analysis and the 1,000,000-year analysis is due to seepage rate averaging. For both durations, the total annual amount of seepage that reaches the repository during the glacial-transition climate is the same. However, the seepage fraction for the 1,000,000-year analysis increases; therefore, the average annual seepage rate per waste package in the seeping environment during the glacial-transition climate decreases. This decrease in the average seepage rate between durations is proportional to the increase in the seepage fraction. This behavior is not observed for the average rates presented over all waste package locations because the number of waste packages in the repository does not change between the two durations.

Table 4. Distribution of Epistemic Uncertainty in the Repository-Wide Average Seepage Rates and Seepage Percentages for 10,000 Years of Non-collapsed Drift Conditions

Parameter	Seepage Rate (m^3/yr/waste package) Glacial-Transition Climate		Seepage Percentage (%) Glacial-Transition Climate		Seepage Fraction
	All Waste Packages	Seep Only	All Waste Packages	Seep Only	
Lower Bound	0.00137	0.0274	0.259	3.95	0.0146
5th-Percentile	0.00271	0.0409	0.554	7.87	0.0423
25th-Percentile	0.00980	0.0600	1.97	11.8	0.150
Median	0.0216	0.0873	4.03	15.3	0.289
75th-Percentile	0.0619	0.175	8.62	19.3	0.464
95th-Percentile	0.226	0.376	18.2	26.8	0.696
Upper Bound	0.549	0.631	27.5	34.4	0.870
Mean	0.0556	0.134	5.92	16.1	0.313

Table 5. Distribution of Epistemic Uncertainty in the Repository-Wide Average Seepage Rates and Seepage Percentages for 1,000,000 Years of Non-collapsed Drift Conditions

Parameter	Seepage Rate (m^3/yr/waste package) Glacial-Transition Climate		Seepage Percentage (%) Glacial-Transition Climate		Seepage Rate (m^3/yr/waste package) Post-10,000-Year Climate		Seepage Percentage (%) Post-10,000-Year Climate		Seepage Fraction
	All Waste Packages	Seep Only	All Waste Packages	Seep Only	All Waste Packages	Seep Only	All Waste Packages	Seep Only	
Lower Bound	0.00137	0.0140	0.259	2.24	0.00438	0.0407	0.680	6.31	0.0327
5th-Percentile	0.00271	0.0251	0.554	4.88	0.00881	0.0766	1.38	12.1	0.0765
25th-Percentile	0.00980	0.0387	1.97	8.14	0.0288	0.112	4.02	17.0	0.230
Median	0.0216	0.0570	4.03	10.8	0.0535	0.154	7.18	20.9	0.396
75th-Percentile	0.0619	0.144	8.62	15.7	0.122	0.285	12.3	25.1	0.565
95th-Percentile	0.226	0.370	18.2	24.3	0.324	0.464	22.7	31.4	0.747
Upper Bound	0.549	0.631	27.5	32.3	0.478	0.592	33.0	38.5	0.870
Mean	0.0555	0.108	5.92	12.3	0.0947	0.204	8.81	21.1	0.400

1.3 SEEPAGE CALCULATIONS FOR SEISMIC FAULT DISPLACEMENT MODELING CASES

The drift seepage abstraction for collapsed drifts (SAR Section 2.3.3.2.3.4.2) is applied for both the 10,000- and 1,000,000-year seismic fault displacement modeling cases.

Table 6 provides the uncertainty range for the repository-wide average seepage rate, seepage percentage, and seepage fraction for the 10,000-year seismic fault displacement modeling case. For each epistemic sample, the repository-wide seepage rate is calculated using Equation 1 and the repository-wide seepage rate for seeping locations is calculated using Equation 2. From these results, the average and selected quantiles are tabulated in Table 6. Table 7 provides the analogous results for the 1,000,000-year calculations. The results, presented in Tables 6 and 7, assume that the fault displacement event that collapses the drift and causes damage to the waste packages occurs before the glacial-transition climate change. In realizations where the fault displacement event occurs after the glacial-transition climate change, the seepage rate up to the time of the event would be a fraction of the non-collapsed drift seepage rate. The factor that would be used to determine the pre-event seepage rate is the ratio of the seepage fractions for non-collapsed drifts to collapsed drifts.

The results in Tables 6 and 7 reveal that the repository-wide average seepage rate is equivalent for the glacial-transition climate when all waste packages are included in the average, but decreases in the 1,000,000-year analysis when only the seeping environment is considered. The reduction in the average seepage rate during the glacial-transition climate between the 10,000-year analysis and the 1,000,000-year analysis occurs because the 1,000,000-year analysis results allocate the same volume of seepage to more waste packages. With the inclusion of the post-10,000-year representation of climate change in the 1,000,000-year analysis, the seepage fraction increases; therefore, due to the inclusion of the post-10,000-year representation of climate change, seepage occurs at locations that had no seepage in the first 10,000 years. In the 1,000,000-year analysis, these locations with zero seepage in the first 10,000 years are included in the seeping environment and the average seepage rate for the glacial-transition climate decreases.

Table 6. Distribution of Epistemic Uncertainty in the Repository-Wide Average Seepage Rates, Seepage Percentages, and Seepage Fractions for 10,000 Years of Collapsed Drift Conditions

Parameter	Seepage Rate (m^3/yr/waste package) Glacial-Transition Climate		Seepage Percentage (%) Glacial-Transition Climate		Seepage Fraction
	All Waste Packages	Seep Only	All Waste Packages	Seep Only	
Lower Bound	0.0365	0.128	7.58	21.5	0.166
5th-Percentile	0.0522	0.143	9.06	22.7	0.237
25th-Percentile	0.0879	0.183	12.4	25.5	0.445
Median	0.144	0.240	17.1	30.2	0.653
75th-Percentile	0.347	0.514	23.6	36.8	0.809
95th-Percentile	0.897	1.19	35.8	42.1	0.927
Upper Bound	1.69	1.77	43.3	45.1	0.980
Mean	0.269	0.390	18.8	31.1	0.617

Table 7. Distribution of Epistemic Uncertainty in the Repository-Wide Average Seepage Rates, Seepage Percentages, and Seepage Fractions for 1,000,000 Years of Collapsed Drift Conditions

Parameter	Seepage Rate (m^3/yr/waste package) Glacial-Transition Climate		Seepage Percentage (%) Glacial-Transition Climate		Seepage Rate (m^3/yr/waste package) Post-10,000-Year Climate		Seepage Percentage (%) Post-10,000-year Climate		Seepage Fraction
	All Waste Packages	Seep Only	All Waste Packages	Seep Only	All Waste Packages	Seep Only	All Waste Packages	Seep Only	
Lower Bound	0.0365	0.101	7.58	17.6	0.0891	0.244	8.81	22.2	0.173
5th-Percentile	0.0522	0.116	9.06	18.8	0.126	0.274	11.2	24.8	0.292
25th-Percentile	0.0879	0.161	12.4	22.0	0.201	0.358	15.9	28.5	0.541
Median	0.144	0.204	17.1	27.1	0.312	0.469	21.5	33.4	0.738
75th-Percentile	0.347	0.469	23.6	31.7	0.596	0.835	28.5	39.8	0.866
95th-Percentile	0.897	1.19	35.8	38.3	1.11	1.26	39.9	44.6	0.948
Upper Bound	1.69	1.77	43.3	44.5	1.44	1.51	47.3	48.7	0.980
Mean	0.269	0.359	18.8	27.6	0.435	0.602	22.9	34.0	0.687

1.4 SEEPAGE CALCULATIONS FOR IGNEOUS INTRUSION MODELING CASE

In the igneous intrusion modeling case, the drift seepage abstraction for non-collapsed drifts is used to determine the number of waste packages in the seeping and non-seeping environments. Prior to the igneous intrusion event, this abstraction is also used to determine the average seepage rate for each waste package group. After the igneous intrusion event, all waste packages in the repository are exposed to a dripping rate that is equal to the average percolation flux for the waste package group (SAR Section 2.3.3.2.4.2.3); therefore, the effective seepage fraction and seepage percentage both become 100% (SNL 2008, Section 6.3.3.1.2). Although the drift seepage abstraction for non-collapsed drifts is used to determine the seepage fraction for placing waste packages into the seeping or non-seeping environments, this placement is only applicable before the igneous intrusion event occurs. Prior to the igneous intrusion event, the seepage conditions in the repository are modeled with the drift seepage abstraction for non-collapsed drifts. After the igneous intrusion event has occurred, every waste package location in the repository, whether in a seeping environment or a non-seeping environment, is exposed to dripping and the applicable abstractions for seeping conditions in the EBS are applied in both the seeping and non-seeping environments. This is modeled by applying dripping specific calculations (e.g., the liquid influx in-package chemistry abstraction) instead of non-dripping specific calculations (e.g., the vapor influx in-package chemistry abstraction), and not by moving waste packages between seeping and non-seeping groups.

For the igneous intrusion modeling case, the effective seepage fraction for both the 10,000- and 1,000,000-year analyses is 100%; therefore, the repository-wide average seepage rate for all waste packages and repository-wide average seepage rate for only those waste packages that experience a liquid flux are the same values. In addition, because the seepage fractions between the two durations are the same, the liquid flux rate during the glacial-transition climate, which is set equal to the average percolation rate for the glacial-transition climate, is the same for both the

10,000-year analysis and the 1,000,000-year analysis. Table 8 provides the uncertainty range for the repository-wide average percolation rate applied as the liquid flux rate in the repository for the 10,000- and 1,000,000-year igneous intrusion cases. The 10,000-year analysis extends the glacial-transition climate to the end of the 20,000-year simulation period and does not apply the post-10,000-year values listed in Table 8. The results presented in Table 8 assume that the igneous intrusion occurs before the glacial-transition climate change; therefore, the reported effective seepage fractions and seepage percentages are 100%. The values in Table 8 do not vary from the lower bound to the median value because the average values of the percolation flux only vary with changes in the infiltration scenario and the 10th-percentile infiltration map is sampled in approximately 62% (see Table 2) of the epistemic realizations.

Table 8. Distribution of Epistemic Uncertainty in the Repository-Wide Average Flux Rate (which is equivalent to the percolation rate) at the Repository Horizon in the Igneous Intrusion Modeling Case for 10,000 Years and 1,000,000 Years

Parameter	Seepage Rate (m^3/yr/waste package) Glacial-Transition Climate	Seepage Percentage (%) Glacial-Transition Climate	Seepage Rate (m^3/yr/waste package) Post-10,000-Year Climate	Seepage Percentage (%) Post-10,000-Year Climate	Effective Seepage Fraction
Lower Bound	0.341	100	0.603	100	100%
5th-Percentile	0.341	100	0.603	100	100%
25th-Percentile	0.341	100	0.603	100	100%
Median	0.341	100	0.603	100	100%
75th-Percentile	0.737	100	1.13	100	100%
95th-Percentile	1.95	100	1.73	100	100%
Upper Bound	1.95	100	1.73	100	100%
Mean	0.610	100	0.892	100	100%

1.5 SEEPAGE CALCULATIONS FOR 1,000,000-YEAR SEISMIC GROUND MOTION MODELING CASE

The drift seepage abstractions for non-collapsed and collapsed drifts are both used to determine seepage conditions for the 1,000,000-year seismic ground motion modeling case (SAR Section 2.3.3.2.4.2.2). As in the other modeling cases, separate seepage rates and seepage fractions are calculated for the waste package groups of each fuel type and percolation subregion combination. Whether the non-collapsed drift abstraction results or the collapsed drift abstraction results are applied depends on the integrity of the drift after each seismic event. In the 1,000,000-year seismic ground motion modeling case, the sequence of seismic events that will occur during each simulation is determined before the seepage calculations are performed. When evaluating the sequence of events, the damage to the drift after each event is calculated and the maximum volume of lithophysal and nonlithophysal rubble that will enter the drift as a result of the events is determined before the seepage calculations are performed. If the maximum volume of lithophysal rubble that collapses exceeds the intact threshold level of 5 m^3/m over the simulated duration, the seepage fraction contribution from waste packages in the lithophysal region is determined from the collapsed drift abstraction results. If the maximum volume of lithophysal rubble does not exceed the 5 m^3/m threshold, the seepage fraction contribution of the lithophysal waste packages is determined from the non-collapsed drift abstraction results. If the maximum volume of nonlithophysal rubble that enters the drift exceeds 0.5 m^3/m over the simulated duration, the seepage fraction contribution of the waste packages in the nonlithophysal region is determined from the collapsed drift abstraction results. If the maximum volume of nonlithophysal rubble does not exceed the 0.5 m^3/m threshold, the seepage fraction contribution of the nonlithophysal waste packages is determined from the non-collapsed drift abstraction results. Although seepage rates for lithophysal and nonlithophysal waste packages may be calculated from different abstractions, the net seepage fraction is still the ratio of the number of waste packages where seepage occurs above the 0.1 kg/yr threshold to the total number of waste packages in the waste package group.

The time history of rubble accumulation in the drift is used to determine the seepage rate from the non-collapsed drift and collapsed drift abstraction results. Table 9 summarizes the implementation.

Table 9. Seepage Model Implementation for Lithophysal and Nonlithophysal Regions for the 1,000,000-Year Seismic Ground Motion Modeling Case

	Seepage Rate		**Seepage Fraction**	
Lithophysal Region	**Rubble Accumulation**	**Seepage Model**	**Total Rubble Accumulation in 1,000,000 Years**	**Seepage Model**
Lithophysal	<5 m^3/m	Non-collapsed drift	<5 m^3/m	Non-collapsed drift
Lithophysal	5 to 60 m^3/m	Interpolated between non-collapsed drift and collapsed drift using rubble accumulation as the interpolation parameter	≥5 m^3/m	Collapsed drift
Lithophysal	≥60 m^3/m	Collapsed drift		
Nonlithophysal	<0.5 m^3/m	Non-collapsed drift	<0.5 m^3/m	Non-collapsed drift
Nonlithophysal	≥0.5 m^3/m	Average percolation flux (no interpolation applied)	≥0.5 m^3/m	Collapsed drift (comparing the average percolation rate to the seepage threshold)

The average seepage rate for each waste package group is the product of the seepage rate from lithophysal locations and the fraction of the waste package group that is in the lithophysal region, added to the product of the seepage rate from nonlithophysal locations and the fraction of the waste package group that is in the nonlithophysal locations. The seepage fraction is calculated similarly.

In modeling cases other than the 1,000,000-year seismic ground motion modeling case, the time variant nature of the seepage rate is due to climate changes and/or the occurrence of an igneous intrusion or a fault displacement event. Due to the time-variant nature of drift degradation, seepage rates in the 1,000,000-year seismic ground motion case change as a function of time. Table 10 provides the uncertainty range for the repository-wide average seepage rates and seepage percentages at the end of the glacial-transition climate and at the end of the simulation.

Table 10 also provides the uncertainty range for the repository-wide average seepage fraction. For each epistemic sample, the repository-wide seepage rate is calculated using Equation 1, and the repository-wide seepage rate for seeping locations is calculated using Equation 2. From these results, the average and selected quantiles are tabulated in Table 10. Figure 1 shows the uncertainty in these seepage rates between the10,000- and 1,000,000-year time points.

The seepage fraction and seepage rate values for the post-10,000-year climate in Table 10 match the values using the collapsed drift abstraction shown in Table 7; this indicates that the drift is fully collapsed by the end of the 1,000,000-year seismic ground motion modeling case. The seepage percentage is not calculated in the TSPA model, but approximate values have been calculated from model results. The percolation flux and seepage rates used to calculate the seepage percentages at 1,000,000 years that are tabulated in Table 10 are consistent with an area for a fully collapsed drift. The glacial-transition values of the seepage rate in Table 10 differ from the fully collapsed values presented in Table 7, indicating that the drift does not fully collapse prior to or during the glacial-transition climate. The seepage percentages in Table 10 for the glacial-transition climate are approximate values because the values are calculated for percolation rates that are applied for a non-collapsed drift. In the 9,000 realizations performed for the seismic ground motion modeling case, the lithophysal rubble accumulation during the glacial-transition climate is less than the threshold value for switching from the non-collapsed drift seepage abstraction in 90% of the realizations. In the nonlithophysal regions, approximately 95% of the realizations accumulate less than 0.5 m^3/m of rubble. Therefore, most of the seepage calculations apply non-collapsed drift seepage during the glacial-transition period. For this reason, approximating the repository-wide seepage percentage using only the non-collapsed drift area during the glacial-transition climate is reasonable.

The average seepage rates for the waste packages in the seeping environment during the glacial-transition climate are lower than the average seepage rates in the seeping environment for the nominal case (see Tables 5 and 10). The reported values do not contradict the expectation that partial drift collapse should lead to higher seepage in the seismic ground motion modeling case. In the seismic ground motion modeling case, the drifts eventually collapse and the seepage fraction for the entire simulation is determined by the collapsed drift abstractions. Since the seepage fraction is higher when the TSPA model invokes the collapsed drift abstraction, the seismic ground motion modeling case places more waste packages into the seeping environment at the beginning of each realization. Therefore, although the total volumetric flow is expected to be higher in the seismic ground motion modeling case than in the nominal case, the average flow in the seismic ground motion modeling case is lower because it is distributed over more waste packages.

Table 10. Distribution of Epistemic Uncertainty in the Repository-Wide Average Seepage Rates, Seepage Percentages, and Seepage Fractions for the 1,000,000-Year Seismic Ground Motion Modeling Case

Parameter	Seepage Rate (m^3/yr/waste package) at the End of the Glacial-Transition Climate		Seepage Percentage (%) at the End of the Glacial-Transition Climate[a]		Seepage Rate (m^3/yr/waste at the End of the Post-10,000-Year Climate		Seepage Percentage (%) at the End of the Post-10,000-Year Climate[b]		Seepage Fraction
	All Waste Packages	Seep Only	All Waste Packages	Seep Only	All Waste Packages	Seep Only	All Waste Packages	Seep Only	
Lower Bound	0.00223	0.00635	0.470	1.72	0.0891	0.244	8.81	22.2	0.173
5th-Percentile	0.00503	0.0132	1.13	2.96	0.126	0.274	11.2	24.8	0.292
25th-Percentile	0.0125	0.0229	3.06	5.50	0.201	0.358	15.9	28.4	0.541
Median	0.0263	0.0377	5.53	8.00	0.312	0.469	21.5	33.4	0.738
75th-Percentile	0.0743	0.0930	9.73	11.5	0.596	0.835	28.5	39.8	0.866
95th-Percentile	0.259	0.308	19.7	20.6	1.11	1.26	39.9	44.6	0.948
Upper Bound	0.580	0.592	29.6	30.3	1.44	1.51	47.3	48.7	0.980
Mean	0.0639	0.0795	7.29	9.50	0.434	0.602	22.9	34.0	0.687

[a] Assumes non-collapsed drift conditions for evaluating the base percolation rate.

[b] Assumes collapsed drift conditions for evaluating the base percolation rate.

(a)

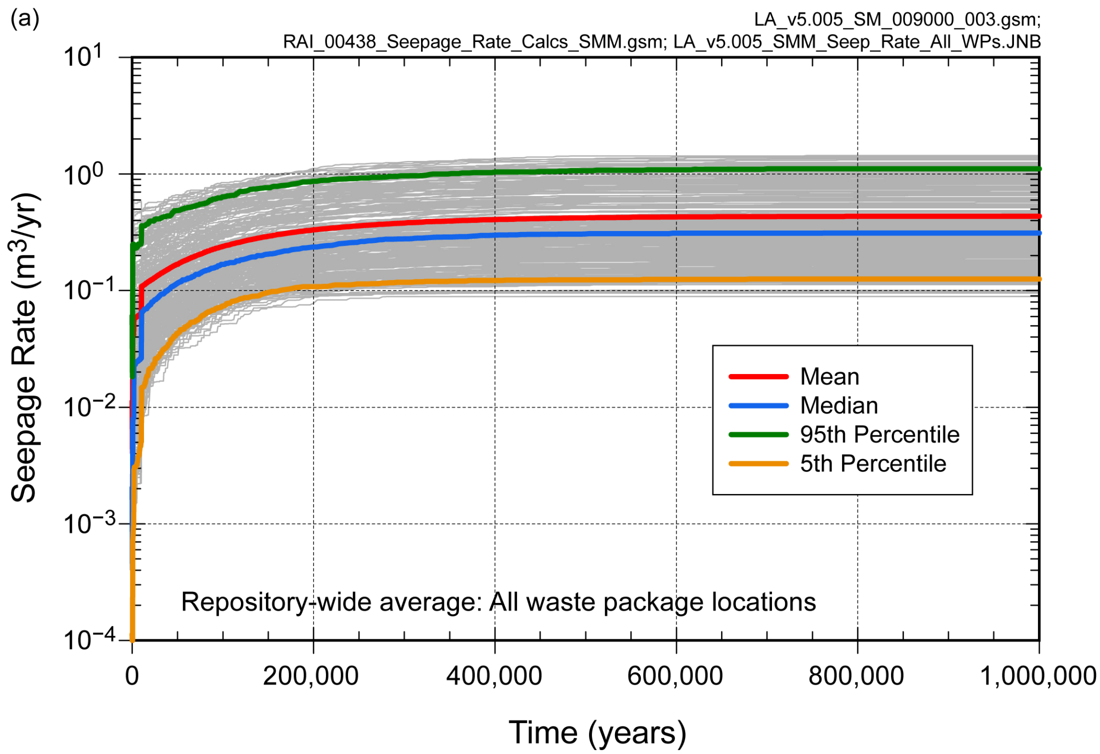

(b)

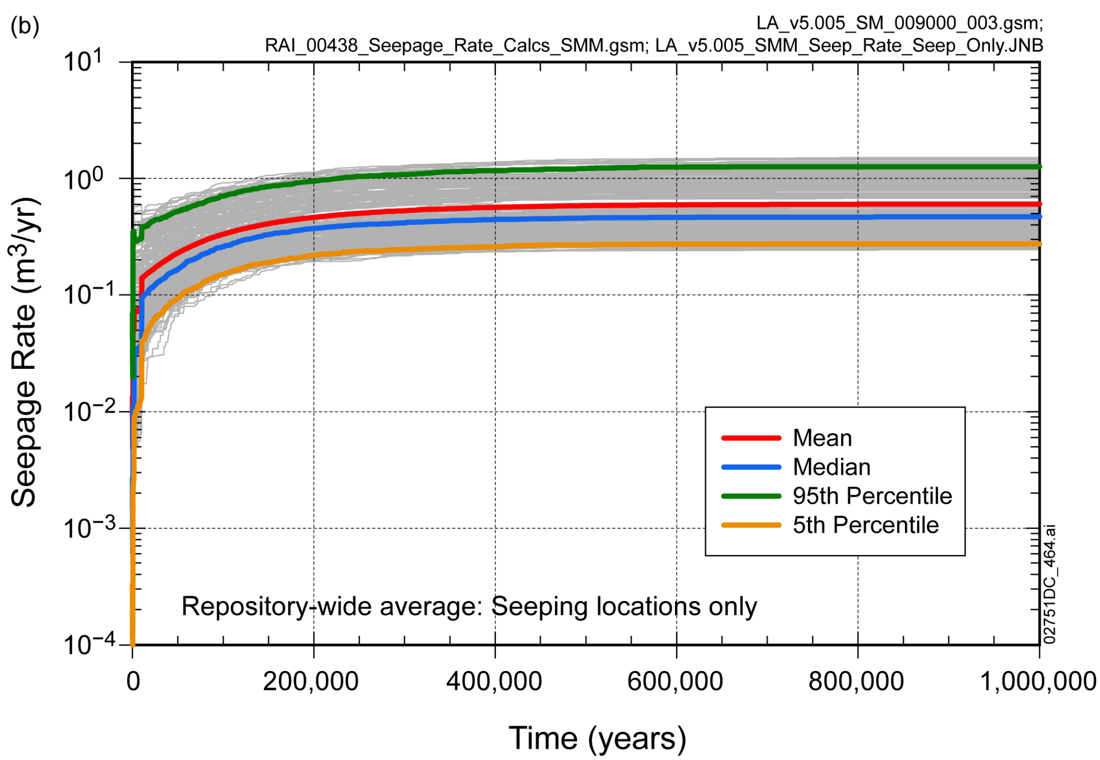

Figure 1. Repository-Wide Average Seepage Rates per Waste Package Location for the 1,000,000-Year Seismic Ground Motion Modeling Case: (a) All Waste Package Locations, and (b) Seeping Locations

1.6 SUMMARY

The uncertainty in the repository-wide seepage rates, seepage fractions, and seepage percentages for the different TSPA modeling cases for 10,000- and 1,000,000-year analyses are reported in Tables 4 through 10. Values are reported for the glacial-transition and post-10,000-year climates for the 1,000,000-year nominal modeling case in Tables 5 and 10, and in Figure 1 for the 1,000,000-year seismic ground motion modeling case. Tables 5 and 10 expand on the mean values represented in SAR Figure 2.1-5. The repository-wide seepage fraction data presented in Table 4 are consistent with repository averages presented in SAR Tables 2.1-6 and 2.1-8, but represent an average over the entire repository, and not a separate average for commercial SNF and codisposal waste packages. Similarly, the seepage fraction values presented in Table 5 are consistent with SAR Table 2.1-7 and the values in Table 10 are consistent with SAR Table 2.1-9.

Tables 4 and 6 present the range of uncertainty for non-collapsed drift and collapsed drift repository conditions, respectively, for the 10,000-year performance period. The differences between the seepage calculations for 10,000 years and 1,000,000 years occur because the 1,000,000-year results include the effects of an additional climate change at 10,000 years.

Uncertainty in the repository-wide seepage rates, seepage fractions, and seepage percentages for the 1,000,000-year seismic fault displacement modeling case is presented in Table 7. For the seismic fault displacement modeling case, the seepage results are presented for a collapsed drift that has a width that is twice the non-collapsed drift width. Table 8 provides the liquid flux rate for both the 10,000- and 1,000,000-year analyses for the igneous intrusion modeling case. This result is equated to the average percolation rate and the values are consistent with the percolation data presented in Table 3.

The repository-wide seepage rates per waste package location for non-collapsed drift and collapsed drift repository conditions can be compared to the results of the example seepage calculations presented in SAR Section 2.3.3.4.2 and shown in SAR Figures 2.3.3-47 and 2.3.3-50. Figure 2 provides a comparison of mean seepage rates between the TSPA results and these sample calculations. Despite using slightly different values for the percolation range, the nonlinearity of the seepage tables, and the uncorrelated samples for epistemic and spatial variability, the results show general agreement. The TSPA results in Figure 2(a) are replicated from Table 5 of the response to RAI 3.2.2.1.3.6-1-005. These results are plotted for four different infiltration scenarios for each climate. The TSPA results in Figure 2(b) are extracted for each infiltration scenario from the set of data that is summarized in Table 7. These results are plotted for four different infiltration scenarios for the monsoon, glacial-transition, and post-10,000-year climates. In the TSPA model, the earliest event modeled in the 1,000,000-year seismic fault displacement modeling case occurs after the climate has transitioned from present day to monsoon; therefore, the present-day climate seepage rate calculated in this modeling case applies the non-collapsed drift abstraction. Although the TSPA model and the example calculations yield similar values, the results are not equivalent. In the sample calculations, the non-collapsed and collapsed drift results are based on sampling epistemic and spatial variability parameters randomly for each climate. Therefore, the mean values for the seepage rate in the example calculation only account for locations where seepage occurs during that climate change. The mean values for the seepage rate from the TSPA model account for locations where seepage occurs during any climate change in the performance period; therefore, the average for any climate may include waste package locations in which no seepage occurs during that climate change. In addition, the sample calculation imposes a different upper limit on the seepage rate for each location. In the sample calculation, the maximum value for the seepage rate at each spatial location is the product of the local percolation flux and the flow focus factor. In the TSPA model results, the spatial variability flow focus factor is not used to determine the maximum seepage rate at individual waste package locations. Despite these differences, the example calculations and the TSPA model results generate comparable values for the seepage rate and the discussion of the sample calculations presented in SAR Section 2.3.3.4.2 is applicable to the TSPA model results as well. This demonstrates that the final results from the TSPA modeling cases appropriately represent the regulatory compliance case.

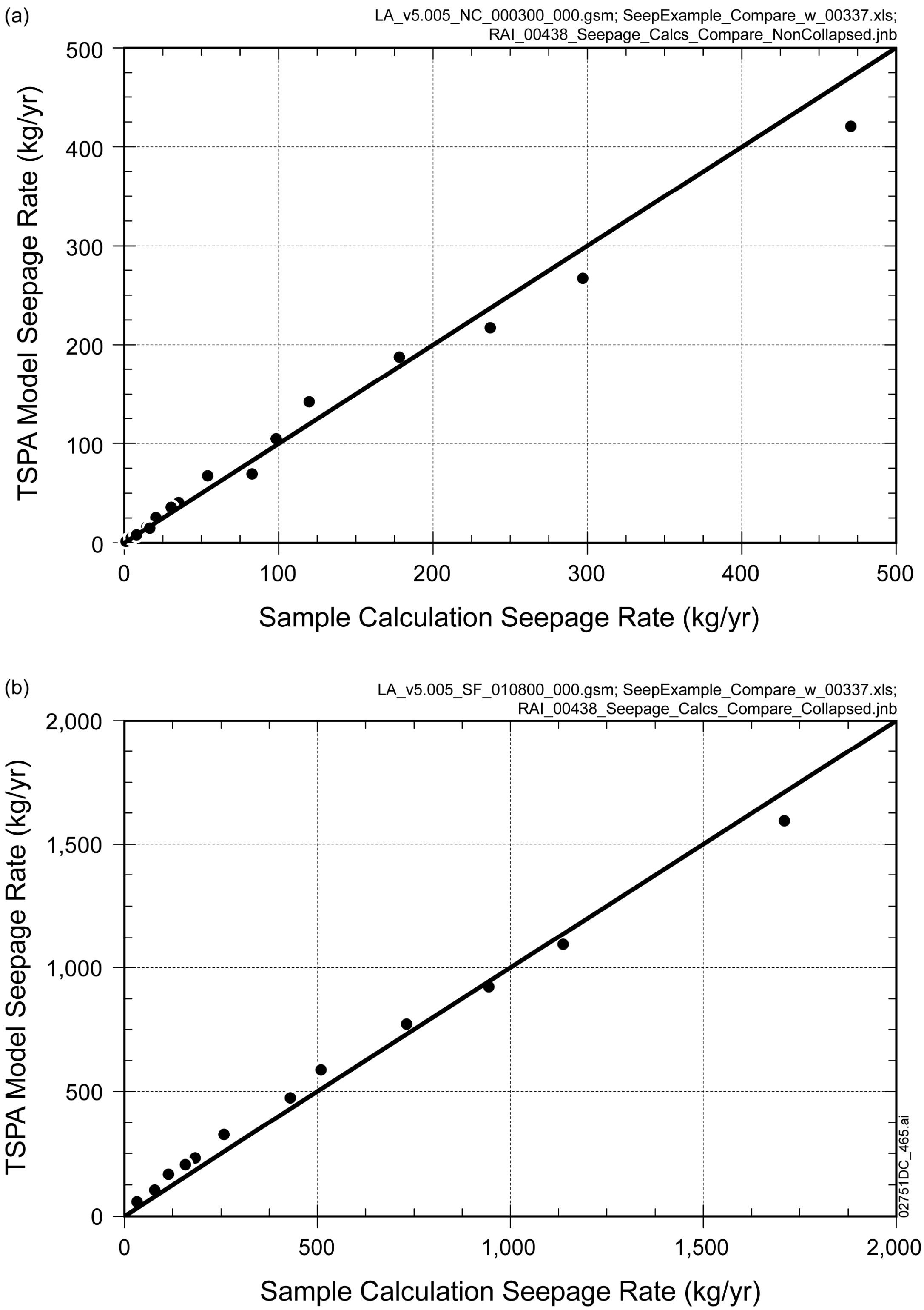

Figure 2. Comparison of Sample Calculations and TSPA Results for the Mean Repository-Wide Average Seepage Rates per Waste Package Location for the 1,000,000-Year Analyses: (a) Non-collapsed Drifts, (b) Collapsed Drifts

2. COMMITMENTS TO NRC

None.

3. DESCRIPTION OF PROPOSED LA CHANGE

None.

4. REFERENCES

SNL (Sandia National Laboratories) 2007. *Abstraction of Drift Seepage.* MDL-NBS-HS-000019 REV 01 AD 01. Las Vegas, Nevada: Sandia National Laboratories. ACC: DOC.20070807.0001

SNL 2008. *Total System Performance Assessment Model /Analysis for the License Application.* MDL-WIS-PA-000005 REV 00 AD 01. Las Vegas, Nevada: Sandia National Laboratories. ACC: DOC.20080312.0001

5. ATTACHMENTS

Attachment 1 – Corrected Table 4 of the Response to RAI 3.2.2.1.3.6-005

Attachment 1 – Corrected Table 4 of the Response to RAI 3.2.2.1.3.6-005

Table 4. Average Percolation Flux Used in the TSPA Calculations

Infiltration Map Percentile[a]	**Climate State**	**MSTHM Percolation at Base of PTn Subregion Rates**[b,c] **(mm/yr)**					**MSTHM Repository Average Percolation at Base of PTn**	
		1 (0.05)	**2 (0.25)**	**3 (0.4)**	**4 (0.25)**	**5 (0.05)**	**(mm/yr)**	**(m^3/yr per waste package)**
10th ***p* = 0.6191**	Present-Day	0.49	2.33	4.32	5.68	6.71	4.09	0.115
	Monsoon	1.23	5.38	8.31	10.00	11.72	7.82	0.219
	Glacial-Transition	0.68	3.72	11.06	20.93	30.46	12.14	0.341
	Post-10,000-year	2.56	15.06	23.32	26.94	30.90	21.50	0.603
30th ***p* = 0.1568**	Present-Day	1.58	6.50	10.84	13.59	15.81	10.23	0.287
	Monsoon	2.34	10.68	17.03	21.24	24.06	16.11	0.452
	Glacial-Transition	2.51	13.53	27.15	38.29	46.90	26.28	0.737
	Post-10,000-year	2.55	17.46	41.50	61.55	77.82	40.37	1.132
50th ***p* = 0.1645**	Present-Day	2.22	9.76~~72~~	15.55	18.87	22.79	14.63	0.410
	Monsoon	2.29	11.22	20.38	26.62	36.14	19.53	0.548
	Glacial-Transition	2.45	15.71	37.17	55.09	69.65	36.17	1.015
	Post-10,000-year	4.29	29.85	55.67	70.47	84.28	51.78	1.452
90th ***p* = 0.0596**	Present-Day	4.942	24.08	36.87	42.53	48.59	34.08	0.956
	Monsoon	12.52	65.45	99.91	115.5	131.51	92.40	2.592
	Glacial-Transition	5.84	40.30	74.93	94.78	113.20	69.69	1.955
	Post-10,000-year	8.81	43.74	66.56	76.91	87.51	61.60	1.728
Mean Results								
	Present-Day	1.21	5.51	9.13	11.28	13.28	8.57	0.24
	Monsoon	2.25	10.76	17.12	20.79	24.81	16.09	0.45
	Glacial-Transition	1.57	9.41	21.69	33.67	44.41	21.74	0.61
	Post-10,000-year	3.22	19.58	34.07	42.51	50.41	31.83	0.89

NOTE: The percolation flux (m^3/yr) was calculated using the cross-sectional area used in the calculation of seepage in the TSPA model (5.5-m drift diameter × 5.1-m waste package length). Mean results for the pre-10,000 year climates are GLUE weighted. Post-10,000 year Mean Results represent the sample mean of the percolation resulting from approximating the distribution of deep percolation by four discrete values. The GLUE weighting factors are used to select these four discrete values.

Source: [a]GLUE probability weighting factors for the 10th, 30th, 50th, and 90th percentile infiltration realizations: SAR Section 2.3.2.4.1.2.4.5.5.
[b]Data extracted from the MSTHM input to the TSPA model, SAR Section 2.3.5.4.1.3.2.
[c]Percolation subregions and quantile ranges SAR Section 2.4.2.3.2.1.2.

RAI Volume 3, Chapter 2.2.1.3.6, Second Set, Number 1:

> Justify the exclusion of the 50^{th} and 90^{th} percentile infiltration prediction calibration property sets from the basis for confidence in site-scale ambient flow model predictions. This information is needed to determine compliance with 10 CFR 63.114(a)(1,2,7).
>
> Basis: SAR Section 2.3.2.5.1 describes confidence building exercises in site-scale unsaturated zone model results using hydrological, thermal, and geochemical observations only for the 10^{th} and 30^{th} percentile calibration property sets. The exercises included: (i) ECRB water potential measurements (SNL, 2007, Section 7.2), (ii) perched water observations in borehole WT-24 (SNL, 2007, Section 7.3), (iii) pneumatic data (SNL, 2007, Section 7.4), (iv) carbon-14 data (SNL, 2007, Section 7.5), and (v) strontium data (SNL, 2007, Section 7.6). Neither the SAR nor the supporting document (which the SAR refers to as SNL 2007a, Section 7) describes validation or confidence building exercises for the 50^{th} and 90^{th} infiltration scenarios.

1. RESPONSE

The 10th and 30th percentile infiltration uncertainty cases are used because these represent the most probable and expected mean infiltration conditions, respectively. In part due to hydrologic calibration, validation to water potential data has low sensitivity to different infiltration uncertainty cases, which is demonstrated by similar results for the 10th and 30th percentile cases. Validation to pneumatic pressure data has low sensitivity to the infiltration uncertainty cases because of calibration and because the effective permeability to air has low sensitivity to infiltration flux over the range of infiltration fluxes investigated, which is also demonstrated by similar results for the 10th and 30th percentile cases. Validations to aqueous strontium and ^{14}C age data, which are sensitive to the infiltration uncertainty cases, show that the data are generally consistent with model results using the 10th and 30th percentile cases. Because the 50th and 90th percentile cases are not representative of the most probable or mean present-day conditions, model results using these cases to predict strontium concentration or ^{14}C age may not match observations. The 50th and 90th percentile cases represent higher infiltration flux conditions that need to be retained to fully capture the effects from infiltration uncertainty, regardless of whether they were used in model validation, or the nature of such model–data comparisons.

1.1 UNSATURATED ZONE FLOW MODEL VALIDATION STRATEGY

One aspect of the unsaturated zone flow model validation is the comparison of model results with recent field observations. As noted in NUREG-1636, the use of field tests for model validation can be limited by uncertainties in initial and boundary conditions. This aspect of using field results as part of the overall model validation strategy was taken into account in the selection of the boundary conditions that were used for validation. Unsaturated zone model results obtained using the 10th and 30th percentile uncertainty cases as boundary conditions for present day infiltration were compared against a variety of measured data from the unsaturated zone. The specific validation data consist of the following: strontium concentration, ^{14}C age, water potential, pneumatic pressure, and perched water thickness. The 10th percentile uncertainty case is used because this is the most probable case, assigned about 61.9% probability of occurring in the total system performance assessment (TSPA) (SAR Section 2.3.2, Table 2.3.2-27). Although the 30th percentile case was assigned a small probability (15.7%), this case has an average infiltration flux over the model domain of 7.96 mm/yr (SAR Section 2.3.2, Table 2.3.2-27). This is close to the probability-weighted average present-day percolation flux (as calibrated using chloride and temperature) over the unsaturated zone flow model domain of 6.7 mm/yr (SAR Section 2.3.2.5.2). The 50th and 90th percentile cases have average infiltration fluxes of 12.28 and 26.78 mm/yr, respectively, over the unsaturated zone model domain (SAR Section 2.3.2, Table 2.3.2-27). Furthermore, the weight for the 90th percentile case is small (6.0%; see SAR Section 2.3.2, Table 2.3.2-27). Accordingly, the 10th and 30th percentile cases are more representative of current field conditions than the 50th and 90th percentile cases because of the revised weights derived through calibration using temperature and chloride data. Therefore these cases are appropriate for use as boundary conditions when comparing unsaturated zone model results with recent observations.

The model results for the different validation data can be grouped according to sensitivity to infiltration flux. Model results for water potential are insensitive to infiltration flux because all infiltration uncertainty cases are calibrated to the same data (see SNL 2007a, Figure 6.2-4). Therefore, the model results for the different uncertainty cases are expected to give similar results. This can be seen in the results for water potential in the Enhanced Characterization of the Repository Block (ECRB) Cross-Drift (SNL 2007a, Section 7.2). This is also the case for the perched water validation, which is based on water potential (SNL 2007a, Section 7.3). Pneumatic validation calculations are insensitive because of calibration and because the effective permeability to air has low sensitivity to the range of infiltration flux in the different uncertainty cases, leading to a similar pneumatic response (SNL 2007a, Section 7.4). Validation using the 10th and 30th percentile cases demonstrates insensitivity to infiltration flux for these data.

Unlike water potential and pneumatic pressure, model results for strontium concentration and ^{14}C age are sensitive to infiltration flux (SNL 2007a, Sections 7.5 and 7.6). Calibration of hydrologic parameters for different infiltration conditions leads to similar model results for water saturation and water potential. However, chemical transport (e.g., strontium and ^{14}C) responds to the fluid flux, which remains different for the different infiltration cases regardless of hydrologic parameter calibration. Note that calibration to chloride data did not result in similar model predictions of chloride concentration for the different uncertainty cases. This calibration was performed instead to assign probabilities for the different uncertainty cases that are consistent with subsurface chloride data.

Validation using the 10th and 30th percentile cases are appropriate boundary conditions because these cases represent the most probable and the average conditions, respectively, that might be expected to match the field inputs (infiltration rates) that produced the field measurements. Results for chloride suggest that the 50th percentile case would not be substantially different than the 30th percentile case and that the lower-probability 90th percentile case would not provide representative results (SNL 2007a, Figures 6.5-1 through 6.5-11). The 50th and 90th percentile cases represent higher infiltration flux conditions that need to be retained to fully capture the effects of infiltration uncertainty, regardless of whether they were used in model validation, or the nature of such model–data comparisons.

1.2 VALIDATION BASED ON STRONTIUM CONCENTRATION IN WATERS

Validation of the unsaturated zone flow model using aqueous strontium concentration is presented in *UZ Flow Models and Submodels* (SNL 2007a, Section 7.6). Strontium is treated as a conservative species in the upper part of the unsaturated zone, but is strongly sorbed in zeolitic rock. Strontium is a common component of natural minerals and frequently substitutes for calcium. It enters the unsaturated zone as a dissolved species; the source of strontium at the ground surface is a combination of strontium dissolved in precipitation and dry deposition of strontium in dust. The strontium flux boundary condition for the strontium model is specified in the same way chloride flux is specified for the chloride model (SNL 2007a, Section 7.6.3). The strontium concentration in percolation is a function of the infiltration flux. Higher infiltration leads to lower strontium concentrations in percolating water. The predicted strontium concentrations using three-dimensional unsaturated zone flow and transport models were compared with data from boreholes USW SD-9 and USW SD-12 and the ECRB Cross-Drift, as shown in Figures 1 and 2 (SNL 2007a, Figures 7.6-1 and 7.6-2). The results are given for the 10th and 30th percentile, present-day, infiltration cases, for two alternative strontium concentrations in infiltrating waters. The two alternative strontium concentrations are labeled in Figures 1 and 2 as “High PD” and “Mid PD” (where “PD” denotes present day) and have strontium concentrations in infiltration water of 14.8 μg/L and 5.8 μg/L, respectively (SNL2007a, Section 7.6.3). Zeolitic rock is only present in significant amounts below the repository and, therefore, is not a factor for the predicted strontium concentrations at the ECRB Cross-Drift. However, USW SD-9 and USW SD-12 penetrate zeolitic rock, and strontium concentrations in these zones are affected by sorption. Model results for the boreholes are computed for two alternative strontium sorption cases to address uncertainty in sorption. Sorption is modeled using a linear equilibrium model with a sorption coefficient, K_d, of 1 m^3/kg or 2 m^3/kg for the cases labeled with “Kdx 2” (SNL 2007a, Section 7.6.3).

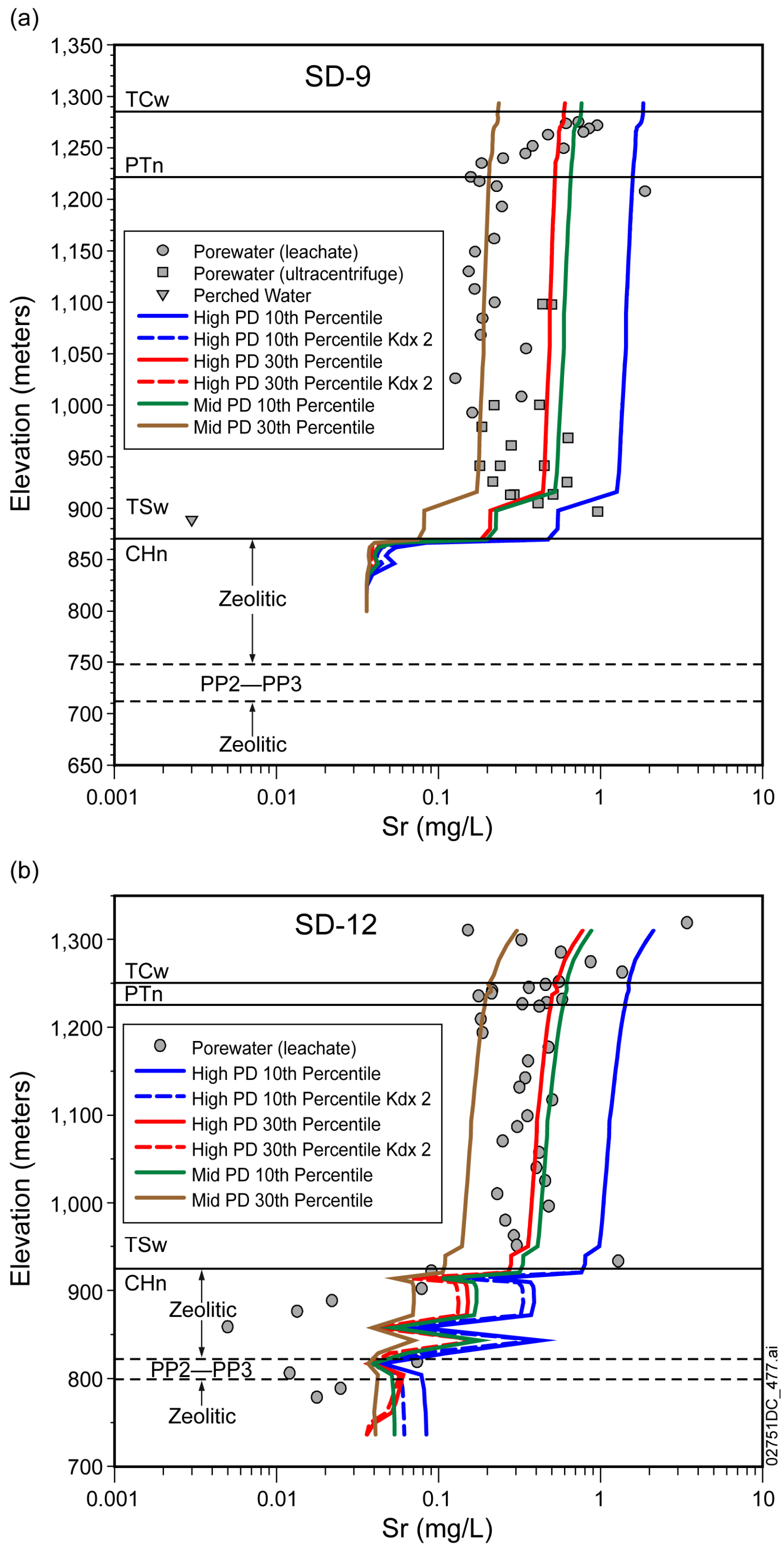

Source: Modified from SNL 2007a, Figure 7.6-1.

Figure 1. Comparison of Measured and Modeled Strontium Concentrations as a Function of Elevation for the Surface-Based Boreholes (a) USW SD-9 and (b) USW SD-12

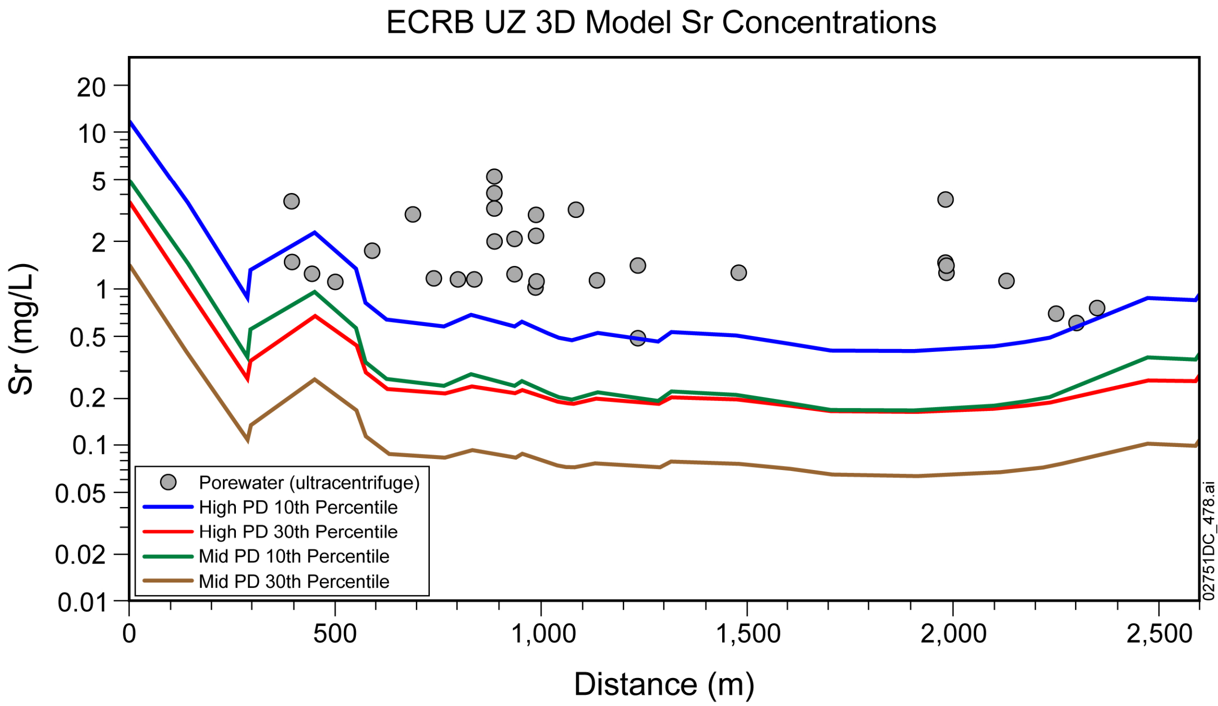

Source: SNL 2007a, Figure 7.6-2.

Figure 2. Measured and Modeled Strontium Concentrations in Pore Waters Extracted from Cores Taken in the ECRB

The average infiltration fluxes for these borehole locations are given in Table 1, which shows that the 30th percentile case has an infiltration flux of more than 2.5 times the 10th percentile case. Both local infiltration fluxes in the unsaturated zone grid cell at each borehole location and average infiltration flux within a 200-m radius of each borehole are shown in Table 1. The 200-m radius was used to approximate one-dimensional unsaturated flow behavior at boreholes for model calibration (SNL 2007b, Section 6.2.5). Averaging over a 200-m radius in the one-dimensional model approximates lateral redistribution of moisture and lateral dispersion of compositional variations over this region. This radius was chosen to represent lateral redistribution in the Paintbrush Tuff nonwelded hydrogeologic unit that occurs in the three-dimensional unsaturated zone flow model (SNL 2007b, Section 6.2.5). Therefore, infiltration flux averaged over a 200-m radius at a borehole may be more representative of transport processes along the borehole than the local infiltration rate at a single grid. For the ECRB Cross-Drift, infiltration fluxes are averaged over 29 grid locations that lie directly above the ECRB Cross-Drift.

From Figures 1 and 2, it is clear that predicted strontium concentrations are lower for the 30th percentile case than for the 10th percentile case. Given the effect of infiltration flux on the strontium concentrations for infiltrating water, higher infiltration fluxes will lead to lower predicted strontium concentrations in general. Average infiltration fluxes at these locations are more than 1.5 times greater for the 50th percentile case than for the 30th percentile case, and more than 3 times greater for the 90th percentile case than for the 30th percentile case.

The results for strontium measured at USW SD-9, USW SD-12, and in the ECRB Cross-Drift indicate that the 10th and 30th percentile cases generally bracket the data except in the zeolitic zone, suggesting that strontium sorption is underestimated. Alternatively, lower strontium concentrations in the deep unsaturated zone may reflect higher infiltration conditions that occurred during the Pleistocene Epoch (SNL 2007a, Section 7.6.3). The relatively small differences in calculated chloride concentrations between the 30th and 50th percentile cases for USW SD-9 and USW SD-12 (SNL 2007a (ERD 04), Figures J-16 and J-17) suggest that calculated strontium concentrations for the 50th percentile case would be similar to the 30th percentile case. However, based on the chloride results, the 90th percentile case is not expected to compare favorably with the data.

Table 1. Average Infiltration Fluxes at USW SD-9, USW SD-12, and the ECRB

	10th Percentile (mm/yr)	30th Percentile (mm/yr)	50th Percentile (mm/yr)	90th Percentile (mm/yr)
USW SD-9 (local)	1.2	3.4	5.8	14.6
USW SD-9 (200-m radius)	2.4	6.9	11.2	26.9
USW SD-12 (local)	0.8	2.2	3.7	8.2
USW SD-12 (200-m radius)	3.2	8.5	12.8	30.6
Average ECRB	3.7	9.9	14.3	34.5

1.3 VALIDATION BASED ON ^{14}C AGE

Validation of the unsaturated zone flow model was also performed using ^{14}C apparent age data from boreholes USW SD-12 and USW UZ-1 (SNL 2007a, Section 7.5). Radiocarbon is created predominantly by atmospheric reactions involving cosmic rays, and the source concentration at the ground surface may be approximated as constant (SNL 2007a, Section 7.5.2). There is no significant mechanism for the creation of ^{14}C within the unsaturated zone (SNL 2007a, Section 7.5.2). Therefore, the concentration of ^{14}C in unsaturated zone waters can be used to quantify the "age" of the water since entering the unsaturated zone.

The ^{14}C model approximates ^{14}C transport as an aqueous-phase process and does not account for gas-phase partitioning or precipitation/dissolution processes. The potential effects of gas-phase partitioning and carbonate mineral precipitation and dissolution are discussed in Section 1.1 of the response to RAI 3.2.2.1.3.7-005. Comparison of ^{14}C model results and data from USW SD-12 are shown in Figure 3.

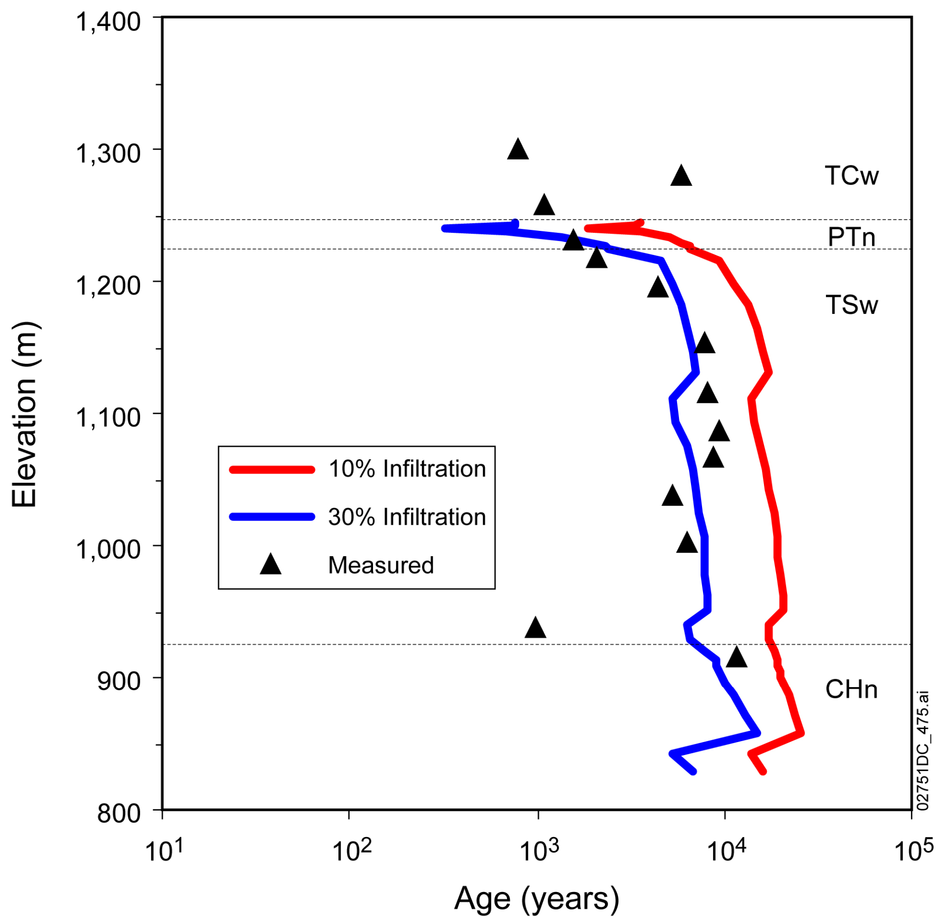

Source: Modified from SNL 2007a, Figure 7.5-2.

Figure 3. Simulated Solute Travel Time of the Matrix Pore Water with Three-Dimensional Simulation for SD-12 Borehole Compared to the Measured ^{14}C Age

Figure 3 shows that the 10th and 30th percentile cases generally approximate the carbon-age data for borehole USW SD-12. Results for USW UZ-1 are shown in Figure 4. The model results for borehole USW UZ-1 generally overestimate the ^{14}C age. Infiltration fluxes for USW SD-12 and USW UZ-1 are given in Table 2.

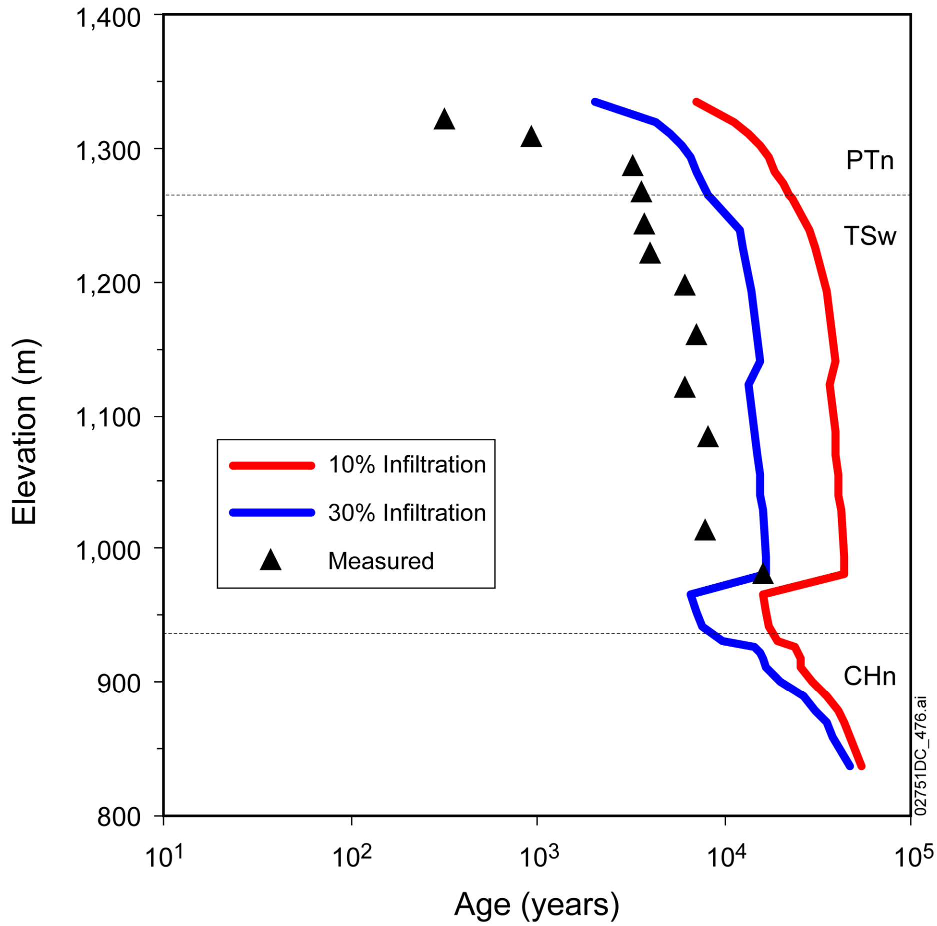

Source: Modified from SNL 2007a, Figure 7.5-1.

Figure 4. Simulated Solute Travel Time of the Matrix Pore Water with Three-Dimensional Simulation for UZ-1 Borehole Compared to the Measured ^{14}C Age

Table 2. Average Infiltration Fluxes at USW SD-12 and USW UZ-1, and the Unsaturated Zone Model Domain

	10th Percentile (mm/yr)	30th Percentile (mm/yr)	50th Percentile (mm/yr)	90th Percentile (mm/yr)
USW SD-12 (local)	0.8	2.2	3.7	8.2
USW SD-12 (200-m radius)	3.2	8.5	12.8	30.6
USW UZ-1 (local)	0.0	0.4	0.1	0.0
USW UZ-1 (200-m radius)	1.8	4.7	6.8	16.1
UZ Flow Model Domain	3.0	8.0	12.3	26.8

.

The local infiltration fluxes correspond to the infiltration fluxes in the grid cell of the unsaturated zone flow model that corresponds to the borehole location. The grid area at USW SD-12 is 12,480 m^2 and the grid area at USW UZ-1 is 12,030 m^2. The 200-m radius infiltration rates are averages over the infiltration model fluxes that are within 200 m of the borehole location. The area within a 200-m radius is about 10 times larger than the local unsaturated zone grid cell area at these boreholes. As can be seen from Table 2, the local infiltration fluxes at USW UZ-12 and USW UZ-1 are smaller than the average infiltration over a 200-m radius around each borehole. The lateral variability in infiltration is greater for USW UZ-1 than for USW SD-12.

Over-prediction of ^{14}C age at USW UZ-1 suggests that lateral flow, lateral dispersion, or local infiltration are underestimated at this borehole. Note that lateral dispersion was not included in the ^{14}C transport model and is, therefore, underestimated (SNL 2007a, Section 7.5.3). A one-dimensional model may provide a better approximation than a three-dimensional model in localized areas with significant spatial variability in infiltration if averaged over a radius representative of lateral mixing caused by lateral flow and dispersion. One-dimensional simulations of ^{14}C age using average infiltration fluxes over the unsaturated zone model domain produced better comparisons with the measured ^{14}C age, particularly for USW UZ-1 (SNL 2007a, Figures 7.5-3 and 7.5-4). The unsaturated zone flow model domain average infiltration fluxes (Table 2) are closer to the 200-m radius average fluxes at boreholes USW SD-12 and USW UZ-1 than the local infiltration fluxes.

The general trend from Figures 3 and 4 is that increased infiltration fluxes lead to lower predicted ^{14}C age. The increases in infiltration fluxes for the 50th and 90th percentile cases at USW SD-12 would lead to predicted ^{14}C ages that are generally lower than the measured ^{14}C ages and would not fit the measured values as well as the 30th percentile case.

For USW UZ-1, the local infiltration flux decreases from the 30th to the 50th and again to the 90th percentile cases while the 200-m average infiltration flux increases monotonically, making interpretations more difficult. Borehole USW UZ-14 lies within the same grid cell of the unsaturated zone model as USW UZ-1. Computed chloride concentrations at USW UZ-14 decrease significantly from the 10th to the 30th percentile case and from the 50th to the 90th percentile cases (SNL 2007a, Figure 6.5-2). However, computed chloride concentrations for the 30th and 50th percentile cases are nearly the same. This suggests that for the three-dimensional ^{14}C age calculation, the 90th percentile case would provide the best match to the data. The one-dimensional validation calculations, both at USW SD-12 and USW UZ-1, show that the 10th and 30th percentile cases are adequate to explain the observations (SNL 2007a, Figures 7.5-3 and 7.5-4). Results from the one-dimensional simulations suggest that infiltration fluxes associated with the 50th and 90th percentile cases, shown in Table 2, would not lead to improved comparisons between model predictions and measurements.

1.4 SUMMARY

Model validation in *UZ Flow Models and Submodels* (SNL 2007a) addresses the 10th and 30th percentile cases because they represent the most probable and the average boundary conditions, respectively, that are expected to match the field conditions (infiltration) associated with field observations used for comparison. Validations based on water potential, perched water, and pneumatic pressure, are relatively insensitive to infiltration and percolation flux. Some of this insensitivity is a result of model calibration for the different infiltration cases. Validations based on strontium and ^{14}C age are sensitive to infiltration flux. For strontium concentration and ^{14}C age, the 50th percentile case is expected to produce results that are not substantially different than the 30th percentile case, based on comparisons of predicted chloride concentration in the unsaturated zone (SNL 2007a, Sections 6.3 and 6.5). The 90th percentile case is not expected to be representative of measured strontium concentrations or ^{14}C age at USW SD-12 based on the same comparisons. Results for ^{14}C age at USW UZ-1 are ambiguous because it appears that the 90th percentile case from the three-dimensional model may provide the best match to the data, while the 30th percentile case from the one-dimensional model provides a close match to the data.

Although the 50th percentile and 90th percentile infiltration uncertainty cases have not been used in validation, they are still expected to be representative of lower-probability conditions for present-day climate, and as such, have been included in the TSPA to fully capture the uncertainty. This disposition would not be influenced by further validation with the 50th and 90th percentile cases.

2. COMMITMENTS TO NRC

None.

3. DESCRIPTION OF PROPOSED LA CHANGE

None.

4. REFERENCES

SNL (Sandia National Laboratories) 2007a. *UZ Flow Models and Submodels*. MDL-NBS-HS-000006 REV 03 AD 01. Las Vegas, Nevada: Sandia National Laboratories. ACC: DOC.20080108.0003; DOC.20080114.0001; LLR.20080414.0007; LLR.20080414.0033; LLR.20080522.0086; DOC.20090330.0026[a].

SNL 2007b. *Calibrated Unsaturated Zone Properties*. ANL-NBS-HS-000058 REV 00. Las Vegas, Nevada: Sandia National Laboratories. ACC: DOC.20070530.0013; DOC.20070713.0005; LLR.20080423.0015; LLR.20080527.0082.

NOTE: [a]Provided as an enclosure to letter from Williams to Sulima, dtd 06/1/09, “Yucca Mountain – Request for Additional Information – Safety Evaluation Report, Volume 3 – Postclosure Chapter 2.2.1.3.6 – Flow Paths in the Unsaturated Zone, Set 1 – (Department of Energy’s Safety Analysis Report Sections 2.3.2 and 2.3.3).”